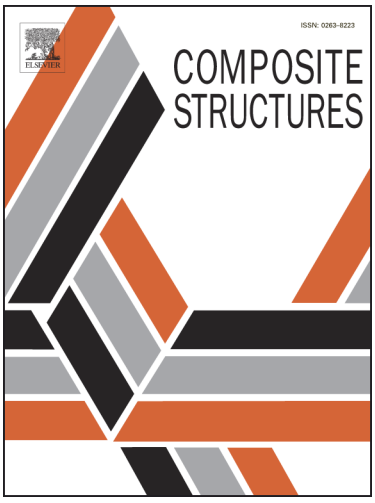

Wave propagation in mass embedded and pre-stressed hexagonal lattices

Danilo Karlčić, Milan Cajić, Tanmoy Chatterjee, Sondipon Adhikari

PII: S0263-8223(20)33013-0
DOI: https://doi.org/10.1016/j.compstruct.2020.113087
Reference: COST 113087

To appear in: *Composite Structures*

Received Date: 9 July 2020
Accepted Date: 1 October 2020

Please cite this article as: Karlčić, D., Cajić, M., Chatterjee, T., Adhikari, S., Wave propagation in mass embedded and pre-stressed hexagonal lattices, *Composite Structures* (2020), doi: https://doi.org/10.1016/j.compstruct.2020.113087

Wave propagation in mass embedded and pre-stressed hexagonal lattices

Danilo Karličić [a,b], Milan Cajić [b,*], Tanmoy Chatterjee[a], Sondipon Adhikari[a]

[a] *College of Engineering, Swansea University, United Kingdom*
[b] *Mathematical institute of the Serbian Academy of Sciences and Arts, Kneza Mihaila 36, Belgrade, Serbia*

Abstract

This paper investigates the elastic wave propagation, mode veering, and in-plane vibration of pre-stressed hexagonal lattice embedded in an elastic medium and composed of axially loaded Timoshenko beams with attached point masses. The frequency band structure of the lattice system is obtained by solving the corresponding eigenvalue problem based on the Bloch theorem and the finite element method. The parametric study is performed by investigating the effects of the pre-stress magnitude, stiffness of elastic medium, and attached point masses on the band structure of a lattice unit cell. For simulating the free vibration behavior of the proposed lattices with different topologies, the Hurty-Craig-Bampton method is introduced to reduce the number of degrees of freedom. Based on the reduced finite element model, the natural frequencies are determined for various boundary conditions. The additional interface reduction technique, called system-level reduction, has been observed to achieve accurate results compared to that of the full model. Numerical experiments demonstrated a significant influence of the additional masses, pre-stress, and stiffness of elastic medium on Bloch waves and eigenvalues of the proposed lattice systems. The effects of different parameters on the emergence of mode veering phenomenon and band gaps are investigated in detail.

Keywords: Embedded Lattices, Attached point masses, Pre-stressed Timoshenko beams, Bloch waves, Hurty-Craig-Bampton method, Veering phenomena.

1. Introduction

A lattice material is an artificially constructed enlarged crystal with carefully tuned properties to attain desired functionality for engineering applications [1]. The concept of lattice materials is naturally inspired by concepts from crystal physics where instead of atoms, lattices are formed by a spatially periodic network of interconnected beams, rods, plates or other slender structures. Their advantage lies in the fact that their unit-cell architecture can be tailored to achieve unique mechanical, elastodynamic or acoustic properties to satisfy specific application demands that may not be achievable with conventional materials. Particularly, periodic [2] and quasi-periodic [3] hexagonal lattice structures may exhibit interesting wave propagation properties in different directions due to its anisotropy, even for shorter wavelengths [4]. Traditionally, lattice structures are classified as two-dimensional (2D) and three-dimensional (3D) lattices. The 2D lattices are formed by filling the plane from a regular polygon while 3D is spatial lattices formed by occupying the space from polyhedra. In this study, only 2D lattice structures are considered and analysed by adopting two different geometries of unit cells. The interesting wave phenomena that appear in such organized structures can lead to the advanced design of artificial materials for wave propagation control using their specific filtering, direction preference, localization or/and polarization properties. It was demonstrated in [2] that for linear waves in two-dimensional lattices, the dispersion relation depends on the orientation of a lattice vector with respect to the wavenumbers. The methods and analytical techniques used in the

*Corresponding author
Email address: mcajic@mi.sanu.ac.rs (Milan Cajić)

analysis of lattice structures apply to periodic materials in general, including phononic crystals and elastic metamaterials.

Some earlier studies demonstrated that in mechanical lattice structures there are intervals of frequencies for which there is no propagation of elastic waves [5, 6]. In some of them two-dimensional periodic structures were considered with phononic band-gap phenomena studied based on the assumption of an infinite linear system and Bloch condition in such a manner that the analysis is restricted to a single unit-cell. Later in [7], plane wave propagation in hexagonal and re-entrant lattices, modelled as an assembly of rigidly connected beam elements, was investigated using the Bloch theorem and finite element method. To study the directional behaviour of hexagonal lattices for varying construction angles, two-dimensional dispersion relations were obtained and analysed. The authors devoted special attention to the determination of phase and group wave velocities. Similarly, a novel design of a honeycomb lattice geometry based on a combination of conventional and auxetic cores is proposed in [8] to improve the band structure of such periodic structures. The computational analyses of bandgap properties of the proposed systems are performed by using a spectral finite element approach combined with Bloch wave boundary conditions and the use of a Wittrick-Williams method [9]. In contrast to Bloch waves analysis of general two-dimensional lattices using approximate methods such as Ritz, finite element or plane wave expansion, an exact wave-based approach is proposed in [10]. The validity of the method is demonstrated on the simple example of an aperiodic bi-material beam, and for more complex examples of the square, diamond, and hexagonal honeycomb lattices. Moreover, in [11] the authors have questioned the applicability of Bloch analysis for band structure investigation of discrete systems with asymmetry. The conclusions from solid-state physics claim that extremum of frequencies exclusively occurs on the boundary of the irreducible Brillouin zone. However, using the new transformation technique and asymmetrical counter-example of honeycomb lattice, the authors have shown that this is not strictly valid for a general wave propagation problem.

Investigating the vibration behaviour of periodic and quasi-periodic lattice beam structures is important for their complete dynamic analysis and potential design of vibration insulators [12–14]. One of the popular methods for analyzing dynamic systems is component mode synthesis (CMS), which is essentially a physics-based sub-structuring and model reduction technique. In general, it operates by modelling the sub-components individually and their reduced dynamic models are assembled to form a global system. Thus, it captures the global dynamic behaviour within a significantly reduced computational effort. This is discussed later in detail (Section 3). The literature related to CMS methods is well developed and they have been utilized to solve structural dynamic problems over the past few decades. Extensive reviews of CMS methods can be found in [15, 16]. However, their usefulness for analyzing periodic structures has only been explored recently. Few applications of CMS in analyzing periodic structures are as follows: Dynamics of two gradient honeycomb structure was investigated in [17] by considering the full-scale finite element model with CMS sub-structuring to determine the frequency response functions (FRF). The wave finite element (WFE) and Craig-Bampton method were used for assessing the harmonic response of coupled mechanical systems that involve one-dimensional periodic structures and coupling elastic junctions in [18]. A numerical approach was proposed in [19] to compute the dynamic response of periodic structures with cyclic symmetry, and assemblies made up of periodic structures. An efficient topology optimization method for periodic structures with static condensation was developed in [20] such that the macrostructure is identically partitioned into several scale-related sub-structures represented by the zero contours of a level set function.

The vibration transmission and isolation properties of the tri-chiral lattice structure was studied in [21] for the uniform and gradient types of geometry parameters. The finite element method in conjunction with the Bloch theorem was employed to analyse the band structure and identify the corresponding stop and passbands. Moreover, by considering the full finite element model of the lattice structure, the harmonic response is estimated and significant attenuation in the vibration transmission is found with the width corresponding to the frequency range of bandgap region. In [22], the authors observed an important problem of the in-plane impact and dynamic response of

the gradient hexagonal lattice by studying the deformation modes and energy absorption capacity in details. By considering the strain gradient elasticity theory and homogenization technique, the band buckling and vibration of a two-dimensional triangular lattice and a sandwich structure based on the Euler-Bernoulli and Timoshenko beam theories were studied in [23]. It is found that the bending rigidity, critical buckling load and natural frequency are strongly affected by the lattice microstructure properties and these dependencies are captured by the generalized simple beam model. On the other hand, in [24] the authors have analysed the base excited beam-like periodic lattice structure with internal resonators, where the model exhibits high stiffness and damping. It was demonstrated that for the specially designed geometry based on chiral topology, the system can be in resonance at selected frequencies with vibration attenuation capabilities obtained over desired frequency ranges.

Investigations in the previously mentioned studies mostly relied on dynamic models and Bloch wave analysis of bandgap and directional behaviour properties of cellular lattices. The other methodologies to study the dynamic behaviour of periodic solids includes homogenization techniques, which yield an equivalent continuum representation with the information about the properties and geometry of the unit cell. Among these techniques, there are several approaches but two major directions applied in lattice structures include numerical multiscale methods [25] and asymptotic expansion methods [26, 27]. Another class of lattice structures that excludes Bloch analysis belongs to strongly nonlinear periodic lattices, where suitable methods for nonlinear differential equations are used to calculate amplitude-dependent dispersion curves [28, 29]. The hierarchical [30] and undulated [31] structural lattices are also studied in the literature using finite element method and Bloch theory [31]. However, the aforementioned analyses are out of the scope of this research and are not detailed here.

Pre-stress effect introduced into the lattice beam elements can boost the bandgap properties by controlling the dispersion characteristics through the alternation of the structural effective stiffness. Such pre-stressed beams assembled in the hexagonal lattice are investigated in [32], where finite element method and Bloch's theorem are employed to generate dispersion curves. This effect is also examined on dispersion diagrams for the axial and flexural waves in quasi-periodic infinite beam structures [33]. It was noticed that a tensile axial pre-stress causes a length reduction of passbands by leaving the length of stop-band intervals almost unaltered. More general analysis of periodic and quasi-periodic structures can be found in [34–36].

The literature on periodic Timoshenko beams based lattice structures without [9, 37] and with pre-stress [36, 38, 39] is sparse and as per the author's knowledge, there is no work addressing the problem of lattice structures with pre-stressed Timoshenko beams embedded in elastic medium and with attached point masses. A few studies investigated the veering of dispersion branches in waveguides [40] and lattice structures [4, 7, 41–43]. According to [44], mode localization phenomenon has often been observed in periodic structures [45–47], where small disturbances in the periodicity may lead to the confinement of one or more vibration modes to some small regions. Mode veering can also occur in non-conservative mechanical systems with dissimilar components [48, 49]. Moreover, in [50], the authors studied the emergence and disappearance of veering, cut-off/cut-on, and branch overtaking phenomena in periodic structures with various topologies representing microtubule-like networks. They also investigated the effect of damping and analysed both in-plane and out-of-plane motions as well as dependence between their modes. Very recently, close mode approximation in near-periodic structures was investigated in [51]. Therefore, the analysis of mode veering phenomenon is significant for practical applications since mode localisation can cause unexpectedly high levels of response in periodic structures, as shown in the first experimental study [52]. In general, this study shows that this phenomenon plays an important role in the analysis of dispersion curves as demonstrated on the frequency band structure determined for the reduced model of the lattice structures. Some studies [4] reported that the mode veering phenomenon comes from the weak modal coupling in the system but such kind of analysis is not elaborated in this work.

Motivated by the lack of studies that address more complex lattice systems, we have sought to study the dynamic and band structure analysis of hexagonal lattice systems embedded in the elastic medium with attached point masses and beam elements subjected to pre-load at the same time.

The finite element method and Bloch theorem are utilized to determine dispersion curves while finite element and reduction technique are used for dynamic analysis. The suggested design results in different band structure and dynamic behaviour of hexagonal lattices that can be tuned only by changing the parameters such as the value of point masses, pre-load magnitude or stiffness of the surrounding medium and without changing the topology of the lattice itself. This is demonstrated through a comprehensive parametric study, where the effects of different parameters on the appearance or disappearance of higher/zero-frequency band gaps and mode veering are discussed in details. This paper is organized as follows: the mechanical model of a hexagonal structure composed of interconnected Timoshenko beams surrounded by an elastic medium and included pre-stress effect and point masses is presented in Section 2. The procedure for the Bloch wave solution and the finite element method for obtaining the dispersion relations is outlined. The procedure for generating the model for dynamic analysis of the proposed system with model reduction technique is given in Section 3. The verification study and effect of lattice angle, point masses and pre-stress on dispersion characteristic of the system is discussed in Section 4. Finally, Section 5 summarizes the main contributions and results of this work.

2. Problem formulation

2.1. Mechanical model of a lattice structure

To analyse the free in-plane wave propagation in a two-dimensional periodic structure, a hexagonal type of lattice embedded in an elastic Winkler medium is considered as shown in Fig.1 a). The presented hexagonal structure is formed by a periodically distributed three-pointed star-like unit cells consisting of three rigidly connected pre-stressed beams with attached point masses Fig.1 b). The pre-stress is realized through linear springs placed in the beam's axial direction, which possess compressive or tensile properties with the value N_0. The proposed elastic medium is modelled as a Winkler's medium and it is represented by the parallelly distributed springs with stiffnesses in the axial k_u and transverse k_w directions of the beam. Here, the Timoshenko beam model is adopted by taking into account the shear effects and rotational inertia. The local beam coordinates are adopted in such a way that the $x-$ coordinate is considered along the length of the beam and the $z-$ coordinate is considered along the thickness direction.

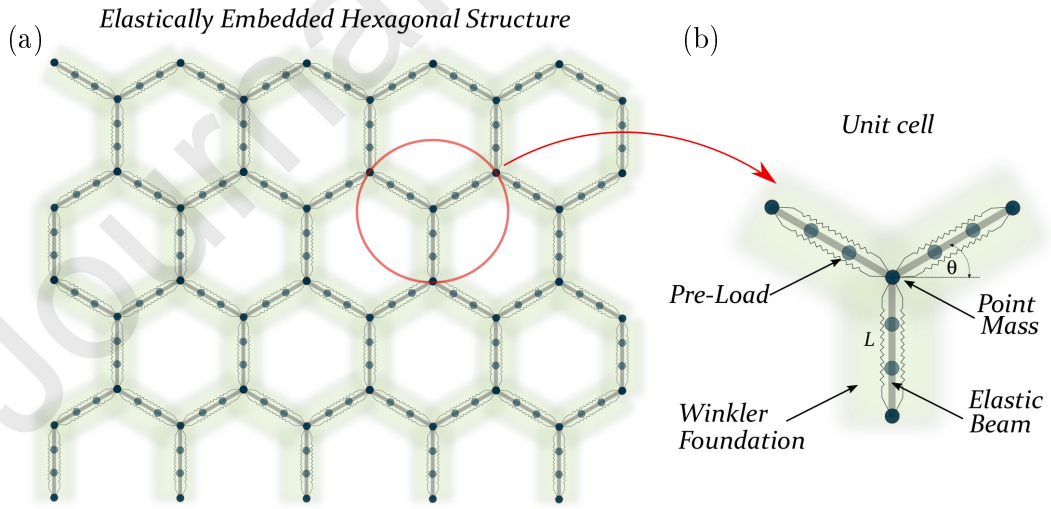

Figure 1: Mechanical model of a hexagonal lattice composed of Timoshenko beams with attached point masses and embedded in an elastic medium, a) two-dimensional hexagonal lattice, and b) three-pointed star shape of a unit cell.

Additional details of the geometrical model of a hexagonal periodic structure unit cell, with its characteristic dimensions and vectors, are given in Fig.2 a). The internal angle of a unit cell is defined as θ. Therefore, by changing the internal angle θ, a hexagonal lattice structure can be transformed into the re-entrant one, where θ can be taken as a negative value. The main geometrical characteristic

of the unit cell is the wall's slenderness ratio defined as $\beta = d/L$. In the literature, the regular hexagonal and re-entrant lattice structures are having internal angles of $\theta = 30°$ and $\theta = -30°$, respectively. As stated before, the hexagonal lattice structures are based on periodically distributed unit cells, where connection nodes are known as lattice points. The vectors defining primitive unit cells and their connection with other unit cells are called basis vectors $(\mathbf{e}_1, \mathbf{e}_2)$, which also defines the direct lattice space [7], as given in Fig.2 a). Therefore, the problem of wave propagation in periodic lattice structures can be reduced to a typical unit cell problem by introducing the periodic boundary conditions according to the Bloch theorem. For the unit cell of the hexagonal lattice structure with positive internal angle θ the basis vectors $(\mathbf{e}_1, \mathbf{e}_2)$ are defined in local Cartesian coordinates with unit vectors $(\mathbf{i}_1, \mathbf{i}_2)$ as

$$\mathbf{e}_1 = (L\cos\theta, L(1+\sin\theta))^T, \qquad (1)$$
$$\mathbf{e}_2 = (-L\cos\theta, L(1+\sin\theta))^T.$$

As mentioned before and based on concepts from the solid-state physics, the lattice points with the corresponding base vectors $(\mathbf{e}_1, \mathbf{e}_2)$ define the direct lattice space, which determines the periodic structure. For such given direct lattice space, one can define the reciprocal lattice space based on the following relation

$$\mathbf{e}_i \cdot \mathbf{e}_j^* = 2\pi\delta_{ij}, \qquad (2)$$

where $\mathbf{e}_j^*$ represents the basis vector of the reciprocal lattice and δ_{ij} denotes Kronecker delta. For the proposed hexagonal lattice structure and unit cell architecture, the reciprocal lattice vectors takes the following form

$$\mathbf{e}_1^* = \left(\frac{1}{2L\cos\theta}, \frac{1}{2L(1+\sin\theta)}\right)^T, \qquad (3)$$
$$\mathbf{e}_2^* = \left(-\frac{1}{2L\cos\theta}, \frac{1}{2L(1+\sin\theta)}\right)^T.$$

In the following sections, the applicability of the proposed concepts will be demonstrated by introducing the Bloch theorem and related periodic boundary conditions.

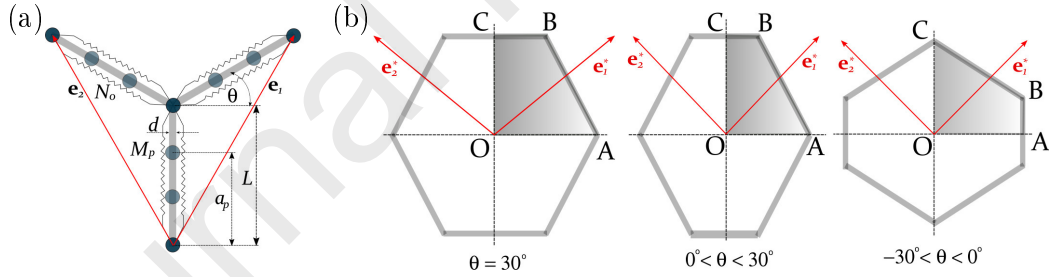

Figure 2: The geometrical characteristics of a unit cell and the first Brioullin zone.

2.2. Bloch's theorem

By assuming the propagation of an elastic wave through an infinite periodic lattice structure formed by tessellating the unit cell along the basis vectors $(\mathbf{e}_1, \mathbf{e}_2)$ and connected through lattice points, this kind of an infinite structure can be reduced by introducing the concept of Bloch theorem and the primitive unit cell. In order to select the proper unit cell, we are going to use the methodology developed for elastic periodic structures [7, 10], where position of the primitive unit cell is determined by the vector $\mathbf{s} = \mathbf{r} + n\mathbf{e}_1 + m\mathbf{e}_2$ placed in the plane of a lattice structure. The set of numbers (n, m) taking the integer values defines the number of unit cells placed along the basis vectors $(\mathbf{e}_1, \mathbf{e}_2)$. Therefore, the vector $\mathbf{s}$ is going from the $(0, 0)$ unit cell until the unit cell defined as (n, m). The vector $\mathbf{r}$ is related to the position of any point inside the reference primitive unit cell defined as $(0, 0)$. Now, according to the Bloch theorem, introducing the displacement vector $\mathbf{w}(\mathbf{r}) = \mathbf{w}_r e^{i\omega t - \mathbf{k}\cdot\mathbf{r}}$ at some arbitrary point inside the reference unit cell corresponds to the wave that propagates at

frequency $\omega(rad/s)$. It should be noted that $\mathbf{w}_r$ is related to the wave amplitude and $\mathbf{k}$ is the wave vector of plane wave. By considering the chosen unit cell determined by the set of numbers (n, m), where n and m are the numbers of unit cells considered in the $\mathbf{e}_1$ and $\mathbf{e}_2$ directions, respectively, the displacement vector of an arbitrary point inside the chosen unit cell is defined as

$$\mathbf{w}(\mathbf{s}) = \mathbf{w}(\mathbf{r})e^{\mathbf{k}\cdot(\mathbf{s}-\mathbf{r})} = \mathbf{w}(\mathbf{r})e^{\mathbf{k}\cdot(n\mathbf{e}_1+m\mathbf{e}_2)}, \tag{4}$$

where $\mathbf{k}\cdot(n\mathbf{e}_1 + m\mathbf{e}_2) = nk_1 + mk_2$.

According to Bloch's theorem [53], amplitude of a propagating wave of a lattice structure without attenuation is independent of a unit cell location within the periodic system. Therefore, elastic wave propagation properties of a periodic system can be completely described by a single representative unit cell with corresponding boundary conditions. Therefore, application of Bloch's theorem can save significant computational efforts and it can be viewed as a kind of (physics-based) model reduction technique applicable to ideally periodic structures. According to Eq.(4), wavenumbers $k_i, (i = 1, 2)$ are complex values given as $k_i = \phi_i + i\epsilon_i, (i = 1, 2)$, where the real part ϕ_i is related to the amplitude attenuation due to wave propagation from one unit cell to another. The imaginary part ϵ_i is related to phase changes across cells and it is known as the phase constant. When analysing the Bloch it is assumed that they are propagating without attenuation since the real part ϕ_i is set to 0. Further, it will be shown how Bloch's theorem is used for setting the periodic boundary conditions in the finite element (FE) model of a unit cell.

To analyse the elastic wave propagation without attenuation, values of the wave vector $\mathbf{k}$ are considered to be imaginary with its values varied within the first Brillouin zone. The concept of Brillouin zone is introduced by considering the reciprocal periodic lattice determined by the vectors defined in Eq.(3), which restricts the value of the wave vector $\mathbf{k}$. According to [7] and [54], the free wave propagation can be reduced to an eigenvalue problem with the frequency of wave propagation determined by varying the parameters (k_1, k_2). The relation between ω and (k_1, k_2) is known as dispersion surface, where each surface is related to a different mode of elastic wave propagation through the periodic structure. To analyse the wave propagation in hexagonal and re-entrant lattice structures, the relation between frequency and wave vector will be determined by considering the Timoshenko beam element and periodic boundary conditions introduced through the Bloch's theorem.

2.3. The equations of motion of an embedded Timoshenko beam

The partial differential equations of motion of the elastically embedded and pre-stressed Timoshenko beam with attached masses are derived by using the Hamilton's principle. Based on the displacement fields of Timoshenko beam and elastic constitutive relation given in [55] the variations of kinetic $\tilde{\delta}K$ and potential $\tilde{\delta}U$ energies are given as

$$\delta K = \int_0^L \left[\rho A\dot{u}\tilde{\delta}\dot{u} + \rho I\dot{\psi}\tilde{\delta}\dot{\psi} + \rho A\dot{w}\tilde{\delta}\dot{w} + \sum_{p=1}^{M} M_p\delta(x-a_p)\dot{u}\tilde{\delta}\dot{u} + \sum_{p=1}^{M} M_p\delta(x-a_p)\dot{w}\tilde{\delta}\dot{w}\right]dx, \tag{5}$$

$$\delta U = \int_0^L \left[EA\frac{\partial u}{\partial x}\tilde{\delta}\frac{\partial u}{\partial x} + EI\frac{\partial \psi}{\partial x}\tilde{\delta}\frac{\partial \psi}{\partial x} + GAk_s\left(\psi - \frac{\partial w}{\partial x}\right)\tilde{\delta}\left(\psi - \frac{\partial w}{\partial x}\right) + k_w w\tilde{\delta}w \right.$$
$$\left. + k_u u\tilde{\delta}u - N_0\frac{\partial w}{\partial x}\tilde{\delta}\frac{\partial w}{\partial x}\right]dx, \tag{6}$$

where $\tilde{\delta}$ is the variation operator and $\delta(x - a_p)$ is the Dirac delta function defining the position of masses on the beam.

Using Eq.(5) and Eq.(6) and Hamilton's principle yields

$$\int_{t_1}^{t_2} (\tilde{\delta}K - \tilde{\delta}U)dt = 0, \tag{7}$$

After partial integration process, the system of partial differential equations for longitudinal and transverse vibrations is obtained as

$$\left[\rho A + \sum_{p=1}^{M} M_p \delta(x - a_p)\right] \ddot{u} - EA\frac{\partial^2 u}{\partial x^2} + k_u u = p(x,t) \tag{8}$$

$$\left[\rho A + \sum_{p=1}^{M} M_p \delta(x - a_p)\right] \ddot{w} + GAk_s\left(\frac{\partial \psi}{\partial \psi} - \frac{\partial^2 w}{\partial x^2}\right) + k_w w + N_0\frac{\partial^2 w}{\partial x^2} = q(x,t) \tag{9}$$

$$EI\frac{\partial^2 \psi}{\partial x^2} - GAk_s\left(\psi - \frac{\partial w}{\partial x}\right) - \rho I\ddot{\psi} = 0 \tag{10}$$

where $u(x,t)$ is the axial displacement, $w(x,t)$ is the transverse displacement and $\psi(x,t)$ is rotation of the cross section. Here, the symbol $\dot{(\cdot)}$ is used to represent $\partial(\cdot)/\partial t$. Material characteristics of the proposed beam model are defined by mass density ρ, modulus of elasticity E, shear modulus $G = E/(2(1+\nu))$ and Poisson ratio ν. The width of a beam is defined with h. The pre-stress of a lattice structure is introduced through axial springs connected to each beam in the lattice and it is denoted by N_0. The stiffness of Winkler's type elastic medium is introduced in $x-$ and $z-$ directions and denoted by k_u and k_w, respectively. The shear correction factor k_s is adopted in the following form $k_s = 10(1+\nu)/(12+11\nu)$, [10]. In this study, the influence of external axial $p(x,t)$ and transverse $q(x,t)$ excitation forces is neglected.

2.4. The finite element model of the unit cell

One of the most applied structural analysis techniques is the finite element method that is often used to obtain the stiffness matrix of the beam. Here, the FE method is introduced to discretize the motion equations of a unit cell with Bloch boundary conditions. The unit cell is modelled as an assembly of rigidly connected Timoshenko beams in the form a three-pointed star, where each limb is represented by a single beam element with attached point masses and surrounded by an elastic medium. Adopted slender ratio starts from $\beta = 1/15$ representing a thick beam model for which effects of shear forces and rotary inertia should be taken into account. Typical finite element models for Timoshenko beam theory are given in [55, 56], where approximations of displacements $u(x,t)$ and $w(x,t)$ and rotation $\psi(x,t)$ are given in the following form

$$u(x,t) = \sum_{j=1}^{6} \Gamma_j(x) q_j(t), \quad w(x,t) = \sum_{j=1}^{6} \Lambda_j(x) q_j(t), \quad \psi(x,t) = \sum_{j=1}^{6} \Theta_j(x) q_j(t), \tag{11}$$

where $\Gamma_j(x), \Lambda_j(x)$ and $\Theta_j(x)$, $(j = 1, 2, ..., 6)$ are the shape functions for six nodal degrees of freedom of Timoshenko beam element given as $\mathbf{q}(t) = [u_1, w_1, \psi_1, u_2, w_2, \psi_2]^T$. The mode shape functions are adopted from [56] and are given in **Appendix 1**. By considering the equations of motion of Timoshenko beam Eq.(8) - Eq.(10), energy variation Eq.(5) - Eq.(7) and approximation of displacements and rotation Eq.(11), the FE model is defined as

$$\mathbf{M}^e\ddot{\mathbf{q}}^e + \mathbf{K}^e\mathbf{q}^e = \mathbf{f}^e, \tag{12}$$

where $\mathbf{M}^e$ and $\mathbf{K}^e$ are mass and stiffness matrices of the beam element while $\mathbf{q}^e$ and $\mathbf{f}^e$ are the corresponding element displacement and force vector, respectively.

By considering a typical unit cell of a hexagonal and re-entrant lattice, the model represents a frame structure where mass and stiffness matrices $(\mathbf{M}^e, \mathbf{K}^e)$ of the beam element are obtained in local coordinates but should be transformed into the global ones. The relations between the local and global mass $\mathbf{M}_g^e$ and stiffness $\mathbf{K}_g^e$ matrices are given by the transformation matrix in the following form

$$\mathbf{M}_g^e = \mathbf{T}^T\mathbf{M}^e\mathbf{T}, \quad \mathbf{K}_g^e = \mathbf{T}^T\mathbf{K}^e\mathbf{T}, \tag{13}$$

in which the transformation matrix is formed as

$$\mathbf{T} = \begin{pmatrix} \mathbf{T}_0 & \mathbf{0} \\ \mathbf{0} & \mathbf{T}_0 \end{pmatrix}, \tag{14}$$

and

$$\mathbf{T}_0 = \begin{pmatrix} \cos\varphi & \sin\varphi & 0 \\ -\sin\varphi & \cos\varphi & 0 \\ 0 & 0 & 1 \end{pmatrix}, \tag{15}$$

where $\mathbf{T}_0$ is the rotation matrix and φ is the angle between the local and global axial directions of the beam as shown in [55]. The three beam model of the chosen unit cell (n, m), connected under different angles according to the local coordinate system, can be assembled by considering matrices from Eq.(13) as follows

$$\mathbf{K} = \mathop{\mathcal{A}}_{e=1}^{n_{ele}} \mathbf{K}_g^e, \quad \mathbf{M} = \mathop{\mathcal{A}}_{e=1}^{n_{ele}} \mathbf{M}_g^e, \tag{16}$$

where $\mathbf{M}$ and $\mathbf{K}$ are the global mass and stiffness matrices of the unit cell and n_{ele} is the number of elements in the unit cell. Thus, the FE model of a unit cell is given as

$$\mathbf{M}\ddot{\mathbf{q}} + \mathbf{K}\mathbf{q} = \mathbf{f}. \tag{17}$$

The number of elements (n_{ele}) chosen in discretization of the unit cell is defined in the numerical section.

2.5. Dispersion relations - Periodic boundary conditions

By using the previously described concept, a corresponding eigenvalue problem can be established whose solution gives dispersion curves i.e. frequencies in terms of wavenumbers. Dispersion analysis enables one to detect band gaps at corresponding ranges of frequencies. Therefore, by considering the Bloch wave propagation in a unit cell described by the FE model given in Eq.(17), the dispersion curves can be generated as the solution of the following eigenvalue problem. Introducing harmonic solution $\mathbf{q}(x,t) = \mathbf{q}(x)e^{i\omega t}$ into Eq.(17), yields

$$(\mathbf{K} - \omega^2\mathbf{M})\mathbf{q} = \mathbf{0}\ , \tag{18}$$

where the force vector $\mathbf{f}$ of interaction between cells is neglected and ω is the frequency of free wave propagation. The vector $\mathbf{q}$ of nodal displacements is given in the following form

$$\mathbf{q} = \{\mathbf{q}_0 \quad \mathbf{q}_1 \quad \mathbf{q}_2 \quad \mathbf{q}_i\}^T, \tag{19}$$

where $\mathbf{q}_0, \mathbf{q}_1$, and $\mathbf{q}_2$ are the vectors of nodal displacements at end nodes of the unit cell. The nodal displacements in vector $\mathbf{q}_i$ are related to degrees of freedom of internal nodes of the unit cell. The absence of external forces in internal nodes simplifies the analysis by considering the free wave propagation, which yields a significant reduction in computation time. Based on the Bloch's theorem, the periodic boundary conditions related to the unit cell are applied on the end nodes displacements as follows

$$\mathbf{q}_1 = e^{k_1}\mathbf{q}_0, \quad \mathbf{q}_2 = e^{k_2}\mathbf{q}_0. \tag{20}$$

By using the equation Eq.(20), transformation matrix can be applied to the global vector of nodal displacements as

$$\mathbf{q} = \mathbf{T}_b\mathbf{q}_r, \tag{21}$$

where the global vector of nodal displacements is reduced to $\mathbf{q}_r = \{\mathbf{q}_0 \quad \mathbf{q}_i\}^T$, and matrix $\mathbf{T}_b$ is defined as

$$\mathbf{T}_b = \begin{bmatrix} \mathbf{I} & \mathbf{0} \\ \mathbf{I}e^{k_1} & \mathbf{0} \\ \mathbf{I}e^{k_2} & \mathbf{0} \\ \mathbf{0} & \mathbf{I} \end{bmatrix}. \tag{22}$$

Inserting Eq.(21) into Eq.(18) and pre-multiplying the resulting equation with the Hermitian (complex conjugate) transpose matrix $\mathbf{T}_b^H$, yields

$$(\mathbf{K}_r(k_1,k_2) - \omega^2 \mathbf{M}_r(k_1,k_2))\mathbf{q}_r = \mathbf{0} \ , \tag{23}$$

where mass and stiffness matrices are now given as

$$\mathbf{M}_r(k_1,k_2) = \mathbf{T}_b^H \mathbf{M} \mathbf{T}_b, \tag{24}$$

$$\mathbf{K}_r(k_1,k_2) = \mathbf{T}_b^H \mathbf{K} \mathbf{T}_b.$$

The transformation matrix for the force vector can be found in a similar manner (see [4, 10]).

By solving the eigenvalue problem given in Eq.(23) and varying the values of wave numbers $k_i, (i = 1, 2)$ within the first Brillouin zone, obtained results can be displayed in the form of dispersion surfaces $\omega = \omega(k_1, k_2)$. However, computational effort can be substantially reduced by exploiting the symmetry properties of the first Brillouin zone and a unit cell. From the physical viewpoint, the geometrical shape of the first Brillouin zone is directly dependent on the internal lattice angle θ and it can form a uniquely defined primitive cell in the reciprocal space determined by the vectors $(\mathbf{e}_1^*, \mathbf{e}_2^*)$. One can find more details about the symmetry and Brillouin zone structure in [57, 58]. The reduced part of the first Brillouin zone is known as the irreducible Brillouin zone (IBZ), where for solution of the eigenvalue problem and determination of dispersion curves one should consider values of wavenumbers along the contours only. For hexagonal and re-entrant lattices, the IBZ and its contours are given as shaded regions denoted by $O-A-B-C-O$ (see Fig.2 (b)). However, for the regular hexagonal lattice there is one additional symmetry whose IBZ is given in the first part of (Fig.2 (b)) with its reduced contours $O-B-C-O$. In the following, the formation of a band structure is based on the restricted zone of the IBZ in the reciprocal lattice frame, where coordinates of boundary points are given in Table 1, [9].

Table 1: The boundary points of the irreducible Brillouin zone of hexagonal and re-entrant lattice structures.

Type of periodic structure	Hexagonal structure $0° \leq \theta < 90°$	Re-entrant structure $-30° < \theta \leq 0°$
O	$(0,0)$	$(0,0)$
A	$2\pi(1/(4\sin^2\phi), -1/(4\sin^2\phi))$	$2\pi(1/2, -1/2)$
B	$2\pi(1-1/(4\sin^2\phi), 1/(4\sin^2\phi))$	$2\pi(1-1/(4\cos^2\phi), -1/(4\cos^2\phi))$
C	$2\pi(1/2, 1/2)$	$2\pi(1/(4\cos^2\phi), 1/(4\cos^2\phi))$

To determine the band structure diagrams, values of the wave vector defined in the reciprocal space as $\mathbf{k} = k_1\mathbf{e}_1^* + k_2\mathbf{e}_2^*$, are varied along the contour $O-A-B-C-O$. The eigenvalue problem Eq.(23) is used to detect bandgap regions. The passbands are frequency ranges for which the lattice structure behaves as a wave-guide. On the other hand, the band gap regions are ranges of frequencies at which propagation of waves is stopped. The importance of determining the band structure of lattice structures lies in potential design of wave-filters.

The eigenvalue problem from Eq.(23) is solved by implementing the MATLAB function eig() to obtain corresponding dispersion curves. Also, the mass and stiffness matrices of the unit cells for the whole structure are implemented in MATLAB to analyse the free wave propagation and in-plane vibrations of the embedded lattice structure with attached masses. The complete set of the surface $\omega(k_1, k_2)$ is denoted as the phase constant surface or dispersion surface. The number of dispersion surfaces directly depends on the size of the eigenvalue problem.

3. Dynamic analysis of the lattice structure

In this section, our goal is to (i) reduce the model of periodic lattice structures, (ii) solve the eigenvalue problem and analyse the band structure, and (iii) investigate the resulting mode veering phenomena due to identical/close modes. The presented lattice structure is modelled as a system of

periodically distributed unit cells in two directions forming a rectangular plate with corresponding boundary conditions. The results obtained in this section are presented in the form of eigenvalue curves for the in-plane vibration. In these diagrams one can also detect bandgap regions. In the previous section, the main assumption was that the hexagonal structure should be considered long enough to apply the Bloch's theorem for detection of band gaps. As a consequence, such periodic structural systems may often consist of with thousands or even millions of degrees of freedom (DOFs) obtained by using the FE method. Analysing the global FE model may render the numerical computation process to be time-intensive, if not prohibitive. Therefore, the Hurty-Craig-Bampton method (also referred to as fixed-interface CMS) is employed here, which reduces the initial number of DOFs of the global FE model by dividing into sub-components. Thus, the intention is to capture the overall dynamic behaviour of the full FE model by an equivalent reduced model by entailing significantly less computational cost. Few recent contributions of CMS include [15, 59–61].

3.1. Hurty-Craig-Bampton model reduction

The Hurty-Craig-Bampton model reduction technique is based on sub-structuring the initial (assembled) system into different sub-components and analysing the interior dynamics by considering truncated set of normal modes (eigenvectors), as shown in [62, 63] . Moreover, the interface between (internal) sub-structural components is retained without any reduction. By using this fixed-interface model reduction framework, the presented hexagonal structure is divided into two parts as shown in Fig.3, where the red coloured circles denote the interface between two sub-structures while the grey coloured circles represent the boundary conditions. The initial step of the Hurty-Craig-Bampton

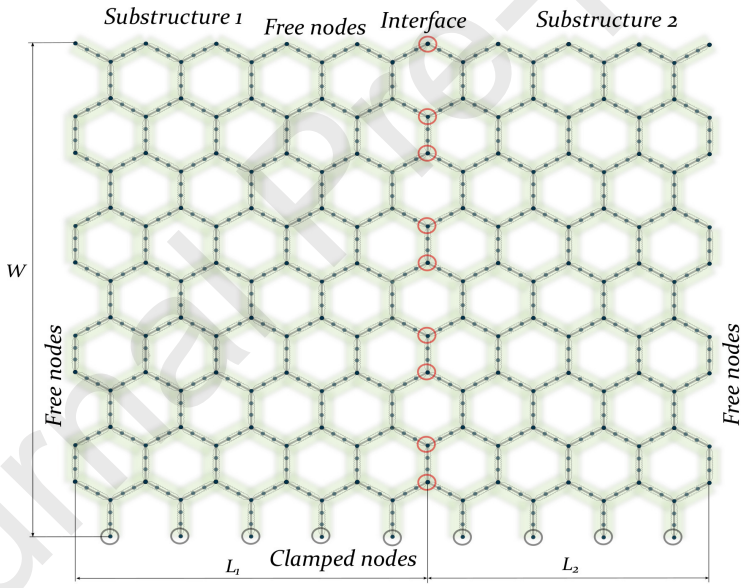

Figure 3: Two sub-structures coupled through the interface in geometrical points.

technique is FE discretization of the equation of motion for p^{th} sub-structure, which gives

$$\mathbf{M}_p\ddot{\mathbf{q}}_p + \mathbf{K}_p\mathbf{q}_p = \mathbf{f}_p, \tag{25}$$

where $\mathbf{M}_p$ and $\mathbf{K}_p$ are the mass and stiffness matrices of sub-structures, $\mathbf{q}_p$ is the nodal displacement vector and $\mathbf{f}_p$ is the forcing vector. Next step is to express the system Eq.(25) into interior and interface (or boundary) DOFs, which is given as

$$\begin{bmatrix} \mathbf{M}_{ii,p} & \mathbf{M}_{ib,p} \\ \mathbf{M}_{bi,p} & \mathbf{M}_{ii,p} \end{bmatrix} \begin{bmatrix} \ddot{\mathbf{q}}_{i,p} \\ \ddot{\mathbf{q}}_{b,p} \end{bmatrix} + \begin{bmatrix} \mathbf{K}_{ii,p} & \mathbf{K}_{ib,p} \\ \mathbf{K}_{bi,p} & \mathbf{K}_{ii,p} \end{bmatrix} \begin{bmatrix} \mathbf{q}_{i,p} \\ \mathbf{q}_{b,p} \end{bmatrix} = \begin{bmatrix} \mathbf{0} \\ \mathbf{f}_{b,p} \end{bmatrix}, \tag{26}$$

The subscripts b and i in the above equations are related to the boundary (or interface) and internal DOFs of the mass and stiffness matrices as well as displacement and force vectors. Following

the methodology proposed in [59, 62], the component modes are formed by determining the static responses corresponding to the internal DOFs, where one of the interface DOF is set as unit displacement while the other DOFs are fixed. From the unit static responses, the set of component modes is formed as

$$\mathbf{q}_{i,p} = -\mathbf{K}_{ii,p}^{-1}\mathbf{K}_{ib,p}, \quad \mathbf{q}_{b,p} = \mathbf{I}, \quad \rightarrow \quad \mathbf{\Psi}_p = \begin{bmatrix} -\mathbf{K}_{ii,p}^{-1}\mathbf{K}_{ib,p} \\ \mathbf{I} \end{bmatrix}. \tag{27}$$

Consideration of this statically reduced model gives sufficiently accurate solutions for the system under static deformation. The obtained component modes ensure a basis for achieving static condensation that holds each interface DOFs and eliminates interior DOFs from the model. The main consequence is that the original physical interface DOFs of a sub-structure are retained, so the system can still be reassembled easily. If only statically obtained component modes are used, they cannot be applied for accurate analysis of the dynamic behaviour of internal DOFs. To extend the analysis and overcame this restriction, the set of component modes should be augmented for the set of dynamical modes that are obtained by fixing the interface DOFs. Taking into consideration the harmonic solution for the internal DOFs from Eq.(26) gives the following eigenvalue problem

$$(\mathbf{K}_{ii,p} - \omega_r^2 \mathbf{M}_{ii,p})\{\eta_{i,p}\}_r = \mathbf{0}. \tag{28}$$

The obtained eigenvectors as the solution of Eq.(28) are known as fixed-interface modes, whereby taking the truncated set of these mass - normalized eigenvectors, they are composed into the fixed-interface mode matrix

$$\mathbf{\Phi}_p = \begin{bmatrix} \{\eta_{i,p}\}_1, ..., \{\eta_{i,p}\}_n \\ \mathbf{0} \end{bmatrix} = \begin{bmatrix} \mathbf{\Phi}_{i,p} \\ \mathbf{0} \end{bmatrix}. \tag{29}$$

Now, by combining the set of component and fixed-interface modes one can form a unique matrix known as Hurty-Craig-Bampton (HCB) reduction matrix given as

$$\mathbf{T}_p^{HCB} = \begin{bmatrix} \mathbf{\Phi}_p & \mathbf{\Psi}_p \end{bmatrix}, \tag{30}$$

The above relation provides a transformation from the HCB generalized DOFs to the sub-structure physical DOFs,

$$\begin{Bmatrix} \mathbf{q}_{i,p} \\ \mathbf{q}_{b,p} \end{Bmatrix} \approx \mathbf{T}_p^{HCB} \begin{Bmatrix} \mathbf{u}_{i,p} \\ \mathbf{q}_{b,p} \end{Bmatrix}, \tag{31}$$

where $\mathbf{u}_{i,p}$ represents the modal coordinate vector associated with the fixed-interface modes.

Introducing the transformed DOFs from Eq.(31) into Eq.(25) and pre-multiplying such obtained results with HCB transformation matrix Eq.(30) yields

$$\mathbf{M}_p^{HCB} = \left(\mathbf{T}_p^{HCB}\right)^T \mathbf{M}_p \mathbf{T}_p^{HCB}, \tag{32}$$

$$\mathbf{K}_p^{HCB} = \left(\mathbf{T}_p^{HCB}\right)^T \mathbf{K}_p \mathbf{T}_p^{HCB},$$

where $\mathbf{M}_p^{HCB}$ and $\mathbf{K}_p^{HCB}$ represents the HCB reduced mass and stiffness matrices, respectively.

After reducing the sub-component matrices one needs to reassemble the whole system to analyse global dynamic behaviour. As mentioned above, the presented hexagonal structure is divided into two sub-structures, where in the case of two parts the following value $p = 2$ is set. Introduction of the coupling matrices that connect displacement vectors of a sub-structure with displacement vectors of the assembly yields mass and stiffness matrices in the following form

$$\mathbf{M}^{HCB} = \sum_{p=1}^{2} \left(\mathbf{R}_p^{HCB}\right)^T \mathbf{M}_p^{HCB} \left(\mathbf{R}_p^{HCB}\right), \tag{33}$$

$$\mathbf{K}^{HCB} = \sum_{p=1}^{2} \left(\mathbf{R}_p^{HCB}\right)^T \mathbf{K}_p^{HCB} \left(\mathbf{R}_p^{HCB}\right),$$

where the reduced matrices $(\mathbf{M}^{HCB}, \mathbf{K}^{HCB})$ represents a sum of the reduced matrices of sub-components. The sub-structure coupling matrices $\mathbf{R}_p^{HCB}$ determined for the hexagonal structure are given in the following form

$$\begin{Bmatrix} \mathbf{u}_{i,1} \\ \mathbf{q}_{b,1} \end{Bmatrix} = \begin{Bmatrix} \mathbf{I} & \mathbf{0} & \mathbf{0} \\ \mathbf{0} & \mathbf{0} & \mathbf{I} \end{Bmatrix} \begin{Bmatrix} \mathbf{u}_{i,1} \\ \mathbf{u}_{i,2} \\ \mathbf{q}_{b,1} \end{Bmatrix} \rightarrow \mathbf{R}_1^{HCB} = \begin{Bmatrix} \mathbf{I} & \mathbf{0} & \mathbf{0} \\ \mathbf{0} & \mathbf{0} & \mathbf{I} \end{Bmatrix}, \tag{34}$$

$$\begin{Bmatrix} \mathbf{u}_{i,2} \\ \mathbf{q}_{b,2} \end{Bmatrix} = \begin{Bmatrix} \mathbf{0} & \mathbf{I} & \mathbf{0} \\ \mathbf{0} & \mathbf{0} & \mathbf{I} \end{Bmatrix} \begin{Bmatrix} \mathbf{u}_{i,1} \\ \mathbf{u}_{i,2} \\ \mathbf{q}_{b,1} \end{Bmatrix} \rightarrow \mathbf{R}_2^{HCB} = \begin{Bmatrix} \mathbf{0} & \mathbf{I} & \mathbf{0} \\ \mathbf{0} & \mathbf{0} & \mathbf{I} \end{Bmatrix}.$$

In further analysis, the reduced mass and stiffness matrices in Eq.(33) are used to determine natural frequencies of the presented hexagonal structure. However, from the literature, it is well known that the interface DOFs can be also reduced and the methodology based on the system-level reduction is introduced next.

3.2. Interface reduction

The system-level reduction is based on the secondary eigenvalue problem of the assembled structure, where the number of interface DOFs is reduced. By dividing the assembled mass and stiffness matrices between the interface and interior parts, and considering only the interface portion, the following eigenvalue problem is formed

$$(\mathbf{K}_{bb}^{HCB} - \omega_r^2 \mathbf{M}_{bb}^{HCB})\{\eta_r^{S-CC}\} = \mathbf{0}, \tag{35}$$

where $\mathbf{M}_{bb}^{HCB}$ and $\mathbf{K}_{bb}^{HCB}$ are the mass and stiffness matrices of the interface part of the assembled structure. The vector $\{\eta_r^{S-CC}\}$ represents truncated set of eigenvectors or S-CC modes. Collecting the S-CC normalized modes into one mode shape matrix yields

$$\mathbf{\Phi}^{S-CC} = \left[\eta_1^{S-CC}, ..., \eta_n^{S-CC}\right]. \tag{36}$$

Transforming the interface DOF of HCB assembled system by using the Eq.(36), the reduced form of S-CC vector is obtained as

$$\mathbf{q}_b \approx \mathbf{\Phi}^{S-CC} \mathbf{u}_b. \tag{37}$$

To derive the S-CC transformed mass and stiffness matrices, pre- and post-multiplication with the extended S-CC modal matrix gives

$$\mathbf{M}^{S-CC} = \left(\mathbf{R}^{S-CC}\right)^T \mathbf{M}^{HCB} \left(\mathbf{R}^{S-CC}\right), \tag{38}$$

$$\mathbf{K}^{S-CC} = \left(\mathbf{R}^{S-CC}\right)^T \mathbf{K}^{HCB} \left(\mathbf{R}^{S-CC}\right),$$

where the extended S-CC modal matrix has the following form

$$\mathbf{R}^{S-CC} = \begin{Bmatrix} \mathbf{I} & \mathbf{0} \\ \mathbf{0} & \mathbf{\Phi}^{S-CC} \end{Bmatrix}.$$

The main drawback of the interface reduction method is small number of interface DOFs since the interface consists of geometrical nodes that are connecting only two sub-structures. However, for efficient computation of large scale periodic structures in low-frequency regime this methodology can be cost-effective and gives results with satisfactory accuracy level.

4. Numerical study and discussion

The band structure of the proposed hexagonal lattice system is investigated for the chosen unit cell configurations based on three coupled elastically embedded Timoshenko beams with attached point masses. Moreover, it is assumed that the beams within the unit cells are pre-stressed and rigidly connected. Two lattice models with different unit cell configurations are adopted in this study known as hexagonal and re-entrant lattices. From the eigenvalue problem formed with mass and stiffness matrices given in Eq.(24) and values of the wave vector $\mathbf{k}$ given along the contour of IBZ, one can obtain corresponding dispersion curves and band structures of the proposed lattice systems. Moreover, the iso-frequency contours of the dispersion surface modes are plotted as functions of wave numbers $\omega(k_1, k_2)$ characterizing the directional wave properties. The effects of the elastic medium, attached point masses, and pre-stress on the frequency band structure and iso-frequency contours are examined in detail. The results from this study are similar to those obtained in [7] when the influences of the elastic medium, attached point masses, and pre-stress are neglected. It should be emphasized that the adopted pre-stress is introduced as a pre-load at each beam of the system. The HCB model reduction technique is introduced to analyse the free in-plane vibrations and corresponding eigenvalue curves of the lattice structure formed for two types of boundary conditions. The main reason for including such reduced model-based investigation was to save additional computational time compared to that of a full model and at the same time ensure that the wave propagation analysis based on a single unit cell can provide satisfactory results of the dynamic behaviour of a lattice system. According to [40], the dispersion phenomena can be divided into two groups such as weak coupling (veering and locking) and strong coupling effects. Which phenomenon, veering or locking, will occur depends on the product of the gradients of dispersion curves at the crossing frequency. Therefore, veering occurs if the group velocities of propagating waves have the same sign while locking appears if their signs differ [40]. In this study, a particular attention is devoted to the analysis of weak coupling effect phenomenon called veering, which occur in eigenvalue problems depending on a variable parameter e.g. stiffness or mass. In the literature, veering phenomenon is usually attributed to the case when two or more curves describing the eigenvalue loci as a function of some variable parameter veer away and diverge instead of crossing. Here, emergence of veering among dispersion curves and frequency curves in terms of stiffness foundation, point masses, pre-load and internal lattice angle is investigated.

4.1. The frequency band structure

The main characteristic of the proposed lattice periodic structure based on the embedded Timoshenko beam-mass system with additional pre-load is that the propagation of Bloch waves and dynamic responses can be controlled by changing only the external pre-load and attached masses without changing the main structural parameters of the lattice structure. Dispersion relations are obtained by varying the wave vector along the contour of the first Brillouin zone. The resulting representation shows the presence of interesting wave phenomena such as mode veering and band gaps. As given above, a common feature of dispersion curves for the hexagonal honeycomb and other types of lattices is the veering of frequencies i.e. convergence and divergence of the eigenvalues, where dispersion curves (dispersion branches) lay close to one another without crossing along the locus $O-A-B-C-O$ in k space. As shown in [7], the shape of the first Brillouin zone changes with the value of the internal angle and there is a significant difference in band structure between lattices with negative and positive internal angles. Therefore, we adopted two interesting cases of lattices with slenderness ratio $\beta = 1/15$ and negative $\theta = -10^\circ$ and positive $\theta = 30^\circ$ internal angles also called re-entrant and regular hexagonal lattices, respectively. In [7] it was demonstrated that a regular hexagonal lattice features both a veering and bandgap phenomena while in the case of re-entrant lattice the later is absent. This study reveals that a number and position of attached point masses can significantly affect the band structure of the system and introduce new band gaps even for re-entrant lattices. From the physical viewpoint, the effect of attached point masses in the proposed lattice system can be characterized as that of internal resonators in the locally resonant

metamaterials [64, 65], which leads to the emergence of new band gaps in the frequency band diagrams. Moreover, the emergence of zero-frequency band gap due to the presence of an elastic medium surrounding the beam elements is demonstrated, thus, causing the appearance of the phenomenon that is often called in the literature as zero-frequency Bragg gap [66]. It is well known that the Bragg band gaps mostly appear at higher frequency branches like in phononic type periodic structures [1, 7, 9].

Some authors [8] used a combination of conventional and auxetic core topology in honeycomb lattices to induce phononic band gaps. However, the lattice structure proposed in this study is a good example where band gaps can emerge at the lowest possible frequency range, starting from the zero-frequency, as a consequence of the elastic medium surrounding the beam elements within the unit cell of a lattice. Moreover, in [67] the authors demonstrated the absence of band gaps in regular hexagonal lattices and doubt about the Bragg scattering nature of band gaps in other types of lattices attributing their generation to localized resonances. In this context, they concluded that in highly connected lattices, the beams themselves act as mechanical resonators enabling the generation of locally resonant band gaps. On the other side, in [68] the authors have shown that resonance frequencies of pinned-pinned beams do not match consistently with directional bandgap frequencies in each direction, therefore suggesting directional band gaps in beam lattice systems are not necessarily linked to local resonance. Such difference of the results between previous studies is attributed to the fact that the latter includes group velocity maps and 3d model considering both the in-plane and out-of-plane modes. An increase in the number of bandgaps at low frequencies caused by the introduced concentrated masses connected to the primary structure of a lattice by soft links was examined in [5]. Some later studies observed locally resonant band gaps induced by microstructure cantilever beams connected to nodes of square [69] and hexagonal [70] lattices. In both studies, besides resonant modes of attached cantilever beams, mass distribution was identified as an important mechanism for bandgap generation. Here, the main goal was to investigate the influences of attached concentrated masses, elastic medium and applied pre-load on the band structure of the proposed lattice systems while elaborating the nature of the resulting band gaps is out of the scope of this study.

Investigation of dispersion curves and their topology, leading to detection of pass and stop bands by using the Bloch wave analysis for a chosen unit cell configuration, is based on a solution of the corresponding eigenvalue problem. This insight into the band structure of the lattice system allows us to passively control elastic wave propagation. In the numerical simulations, the following material and geometrical parameters are adopted unless otherwise specified: the cross-sectional area $A = bh$, the second moment of inertia $I = \frac{bh^3}{12}$ and the wall's slenderness ratio $\beta = L/d = 1/15$. Length of all the beams is $L = 0.125$ m, $\rho = 25 \cdot 10^3$ kg/m^3 is the mass density, $E = 210 \cdot 10^9$ Pa denotes the elastic modulus, $\nu = 0.25$ is the Poisson's ratio and $M = 2$ is the number of attached masses per beam segment. The positions of attached point masses are identical for each beam in the unit cell and they are also placed at the end of each beam i.e. at beam's connection points. The stiffness of Winkler's elastic medium, in which a unit cell of beams are embedded, is $k_u = k_w = 10^6$ N/m^2. The effect of the pre-stress is introduced through the pre-load on each beam within the unit cell as $N_0 = -10^4$ N. In the following, for clear demonstration of the results, the frequency $\omega(k_1, k_2)$ is normalized with respect to ω_0 as $\Omega = \omega/\omega_0$, where $\omega_0 = \frac{\pi^2}{L^2}\sqrt{\frac{EI}{\rho A}}$ is the first flexural frequency of the simply-supported Euler-Bernoulli beam of the length L. The number of finite elements per beam in the unit cell is adopted as $n_{ele} = 25$.

4.2. The effect of attached point masses

The effects of attached masses and internal angle θ on the Bloch wave propagation are investigated by analysing the obtained dispersion curves and corresponding frequency band structure. The dispersion diagrams demonstrate that introduction of additional masses at beams connection points of the lattice can cause a widening of existing or even appearance of new band gaps. Moreover, in some specific frequency range, mode veering phenomenon may appear at several positions on the band structure diagrams. According to [1], for all values of the wave vector k along $O-A-B-C-O$

contour, veering phenomenon occur when two branches are very close one to another without any overlap or crossing. Furthermore, the analysis presented herein is limited to two different lattice structures with the main difference in the internal angle θ. When the angle θ is positive ($\theta = 30°$), the periodic structure is a regular hexagonal honeycomb lattice while for the case when θ is negative ($\theta = -10°$) the periodic structure belongs to the class of re-entrant (auxetic) lattice structures.

Figure 4 shows the frequency band structure diagrams of a regular honeycomb structure for different values of attached point masses and wall's slenderness ratio $\beta = 1/15$. One can count fifteen branches of dispersion curves that correspond to the first fifteen values obtained by solving the eigenvalue problem from Eq.(23). The four different cases are examined starting from the case without attached masses $M_p = 0$ and then introducing and increasing the values of attached masses until $M_p = \frac{1}{2}\rho AL$. A comparison of the results obtained for different values of masses shows quite interesting band structure. It can be noticed that an increase in the attached point masses values leads to the appearance of new band gaps as well as the widening of the existing ones at higher frequencies. Further, for an increase of the values of attached masses, one can observe stretching of dispersion curves that become more flatten, especially curves bounding the band gaps. In comparison to the case without attached masses Fig.4 (a) (see also [7]), where only a single complete band gap is detected for the regular hexagonal honeycomb structure, several band gaps can be detected when masses are attached to lattice nodes followed by widening of band gaps at higher frequencies. As stated in [69], the phononic band gaps are commonly attributed to the destructive interference during the multiple scattering and reflection of elastic waves propagating in periodic materials and structures. It is widely accepted that the location and width of the phononic band gaps are related to the geometrical and material properties of periodic lattice structures. Therefore, band gaps due to destructive interference are strongly affected by the distribution of elastic properties and mass in such materials. In [69], the authors have modified a two-dimensional square lattice by introducing the auxiliary cantilever beams at lattice nodes, which changes the mass distribution within the original lattice structure and induce certain band gaps. Here, similar modifications are taken over regular and re-entrant hexagonal lattice structures by adding only concentrated masses at nodes, which changes the mass distribution inside the lattice but does not introduce locally resonant modes like in the case when microstructure cantilever beams are considered. However, attaching concentrated masses and increasing their values introduces new band gaps (Fig.4 (b) - Fig.4 (d)). These new band gaps are placed between branches that are located at frequencies higher than the bandgap of the corresponding pristine lattice, which can confirm that they are not of local resonance origin. Moreover, one can notice several veering points of dispersion curves in the frequency band diagrams. For example, for all different mass cases in (Fig.4 a) veering between the second and third as well as between the third and fourth branches of the dispersion curve can be observed along the locus O-A. The magnified picture of the veering zone reviles that eigenvalues are close one to another and do not cross but veer away from each other. However, changes in point masses do not affect significantly the number and position of veering points in regular honeycomb lattice structures.

When the wave vector is taken along the entire first Brillouin Zone one can explore the full dispersion surface. For such formed dispersion surfaces one can additionally plot the iso-frequency contour lines as multiple sections of $3D$ dispersion surface. The iso-frequency contours of the regular hexagonal lattice structure given in Fig.5 and Fig.6 are plotted for the first eight frequency branches in a succeeding manner from the lowest to the highest one, and two attached point masses values given as ($M_p = \frac{1}{12}\rho AL$) and ($M_p = \frac{1}{2}\rho AL$). In doing so, the following values of internal lattice angle $\theta = 30°$ and the wall's slenderness ratio $\beta = \frac{1}{15}$ are adopted. If one considers only the iso-frequency contours of the first branch (the first of eight surfaces in Fig.5 and Fig.6), for both lower and higher values of attached masses, it can be noticed that the outward direction of a given iso-frequency line corresponds to the direction of wave propagation at the observed frequency. These contours display lobed features that indicate the anisotropic properties of the lattice structure, which is in line with the results presented in [7]. However, it is interesting to note how the shape of the contours change with an increase of mass. These changes can not be noticed at lower frequency branches while for the higher ones it is obvious that they are significantly modified, which implies differences in the

wave propagation characteristics and mechanical properties between regular hexagonal lattices with different weights of attached masses. This also suggests that if only higher modes are affected then changes in band structure are not caused by the low frequency local resonances but rather ascribed to some other mechanism such as mass distribution within the lattice.

Further, Fig.7 shows the effect of attached masses on the frequency band structure in the case when the internal lattice angle is given as $\theta = -10°$ and the wall's slenderness ratio as $\beta = 1/15$. One can observe fifteen dispersion curves with a single bandgap detected at higher frequency branches. The well-known hypothesis that Bragg band gaps, which are sensitive to changes in lattice spacing, are located at higher frequencies while locally resonant band gaps depending on the presence of resonating elements are narrow and low-frequency band gaps will be corroborated based on the following analysis. It can be noticed that an increase in the value of the attached point masses $M_p = \frac{1}{2}\rho AL$ generates additional narrow and lower frequency band gap. Moreover, in comparison with the results from [7], the example of re-entrant lattice structure shows all the advantages of the proposed design since new band gaps can emerge only by increasing the values of attached masses. It can be noticed that mode veering phenomenon becomes more prominent for lower values of attached masses. However, for higher values of attached masses dispersion curves are more flattened and new band gaps are opened, therefore, reducing the number of veering points in the case of re-entrant lattice structures. This can be easily noticed at higher frequency branches within the locus $O-A-B-C-O$

The iso-frequency contour lines for eight frequency branches and the re-entrant lattice ($\theta = -10°$) with two different values of attached masses are given in Fig.8 and Fig.9. It can be noticed that iso-frequency contours in the first four frequency branches are only slightly changed for the variations of the values of attached masses. However, the effect of an increase of mass is more pronounced at higher frequency branches, where the topology of contour lines is significantly changed concerning the case with lower values of attached masses. Similar to the case with regular hexagonal lattice, these changes implies significant difference in wave propagation properties between two lattice configurations at higher frequency branches.

From the viewpoint of practical applications, the presented iso-frequency contours can be used for analysing the self-collimation phenomenon also called wave-beaming [71]. The self-collimation phenomenon is an alternative way of waveguiding through the periodic medium, where incident wave propagates with almost no diffraction [71]. More details about the application of this phenomenon in the design of mechanical waveguides can be found in [72, 73]. There is a promising potential of lattice structures with attached point masses to be used as waveguides using the self-collimation phenomenon, which can be an interesting subject for some future investigation challenge.

4.3. The effect of Winkler's elastic medium

Fig.10 shows the influence of the stiffness of Winkler's elastic medium on dispersion curves and band structure of the regular hexagonal ($\theta = 30°$) and re-entrant ($\theta = -10°$) lattice structures for the wall's slenderness ratio given as $\beta = 1/15$. The following values of the stiffness of elastic medium are adopted: $k_u = k_w = 0$ N/m^2 and $k_u = k_w = 10^8$ N/m^2. The reason for introducing such high values of stiffness is to obtain the lowest possible band gap known as zero-frequency Bragg gap, as explained in [66]. According to [66], zero-frequency Bragg gaps can appear in periodic structures when structural elements are lying on the elastic foundation, which means that additional stiffness is introduced into the system. Fig.10 (a) and Fig.10 (b) shows the effect of the stiffness of Winkler's elastic medium on dispersion curves determined for the regular hexagonal unit cell. It can be noticed that the band gaps around $\Omega = 4.5$ and $\Omega = 14$ are slightly reduced. However, higher values of stiffness lead to the appearance of the additional band gap near the zero frequency Fig.10 (b). In the case of the re-entrant lattice structure, the effect of change of elastic medium stiffness becomes more prominent since the band gaps at higher frequency branches are even more reduced. In this case, the zero-frequency band gap is also detected. Besides, it is worth noting that dispersion curves are flattened for lower frequency branches and higher values of the stiffness of elastic medium in both cases of regular hexagonal and re-entrant lattice structures. Such behaviour can be physically interpreted as stiffening of the system, where as explained above, re-distribution of elastic properties

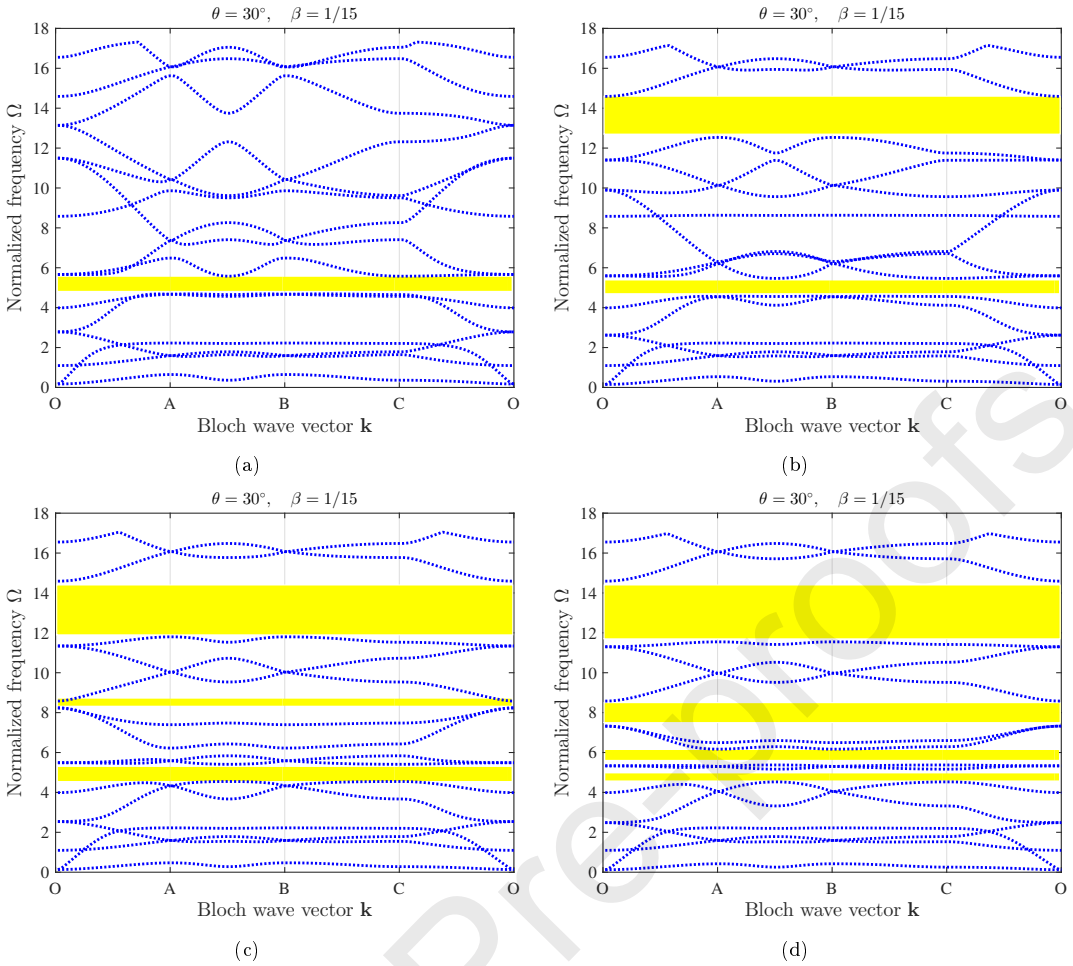

Figure 4: The effect of the attached point masses on the frequency band structures determined for the regular hexagonal $\theta = 30°$ lattice: (a)$M_p = 0$; (b) $M_p = \frac{1}{6}\rho AL$; (c) $M_p = \frac{1}{3}\rho AL$; (d) $M_p = \frac{1}{2}\rho AL$.

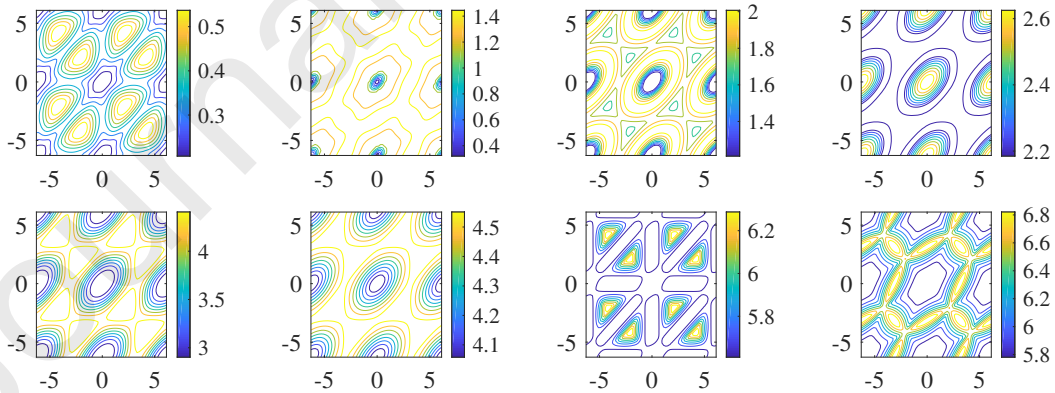

Figure 5: The effect of the attached point masses on the iso-frequency contours of the regular hexagonal, $\theta = 30°$ lattice with additional point masses $M_p = \frac{1}{12}\rho AL$

can contribute to change of band structure properties, which is in this case emergence of the zero-frequency band gap. A number and position of veering points do not change significantly for an increase of foundation's stiffness parameter. However, there is a significant difference between two types of lattices where a lower number of veering points are located within a locus $A - B$ for regular hexagonal lattices, Fig.10 a) and Fig.10 b), while a higher number of veering points can be detected in re-entrant lattices but mostly located between $O - A$ and $B - C$ in Fig.10 c) and Fig.10 d).

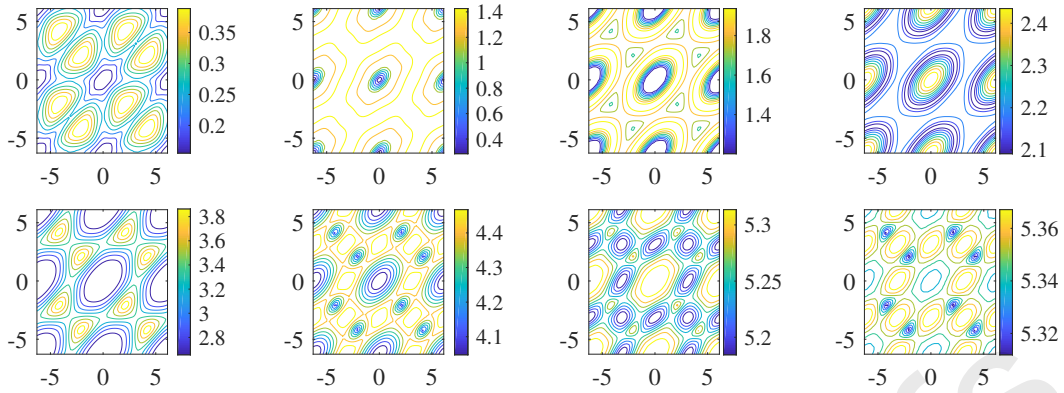

Figure 6: The effect of attached point masses on the iso-frequency contours of the regular hexagonal $\theta = 30°$ lattice with additional point masses $M_p = \frac{1}{2}\rho AL$

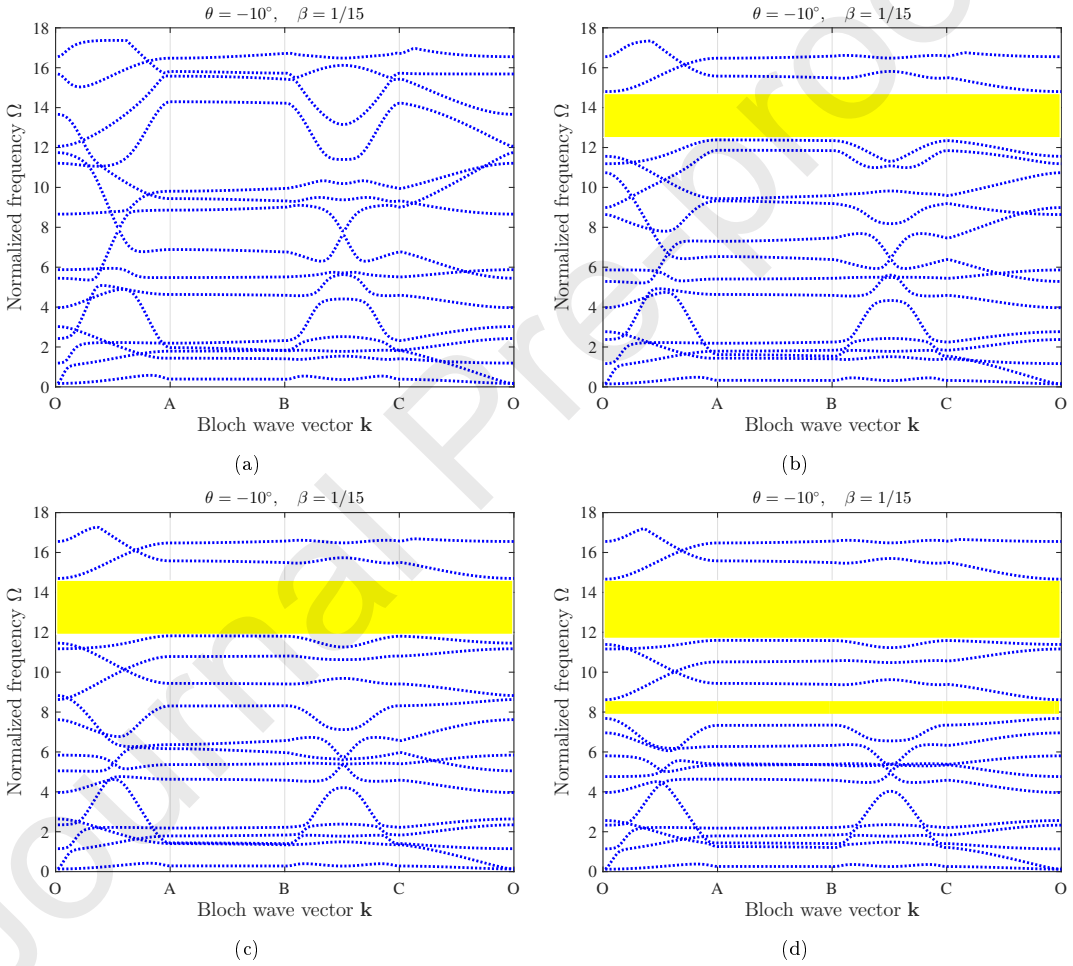

Figure 7: The effect of the attached point masses on the frequency band structures determined for the re-entrant $\theta = -10°$ lattice: (a) $M_p = 0$; (b) $M_p = \frac{1}{6}\rho AL$; (c) $M_p = \frac{1}{3}\rho AL$; (d) $M_p = \frac{1}{2}\rho AL$.

4.4. The effect of pre-load

Fig.11 shows the influence of pre-load on the frequency band structure of the regular hexagonal ($\theta = 30°$) and re-entrant ($\theta = -10°$) honeycomb structures for $N_0 = 0$ and $N_0 = 10^4$ N. The comparative study shows that the effect of pre-load on dispersion curves is small in both cases of honeycomb structures if compared to the effect of other parameters. The main reason for such behaviour might be attributed to the fact that the introduced additional stiffness of the Winkler's elastic medium increases the overall stiffness of the system and therefore, the pre-load does not affect

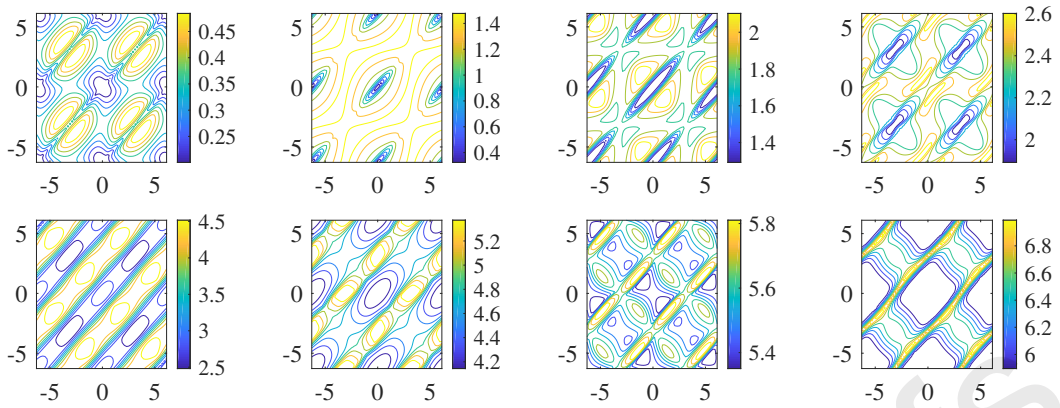

Figure 8: The effect of attached point masses on the iso-frequency contours of re-entrant $\theta = -10°$ lattice with additional point masses $M_p = \frac{1}{12}\rho AL$.

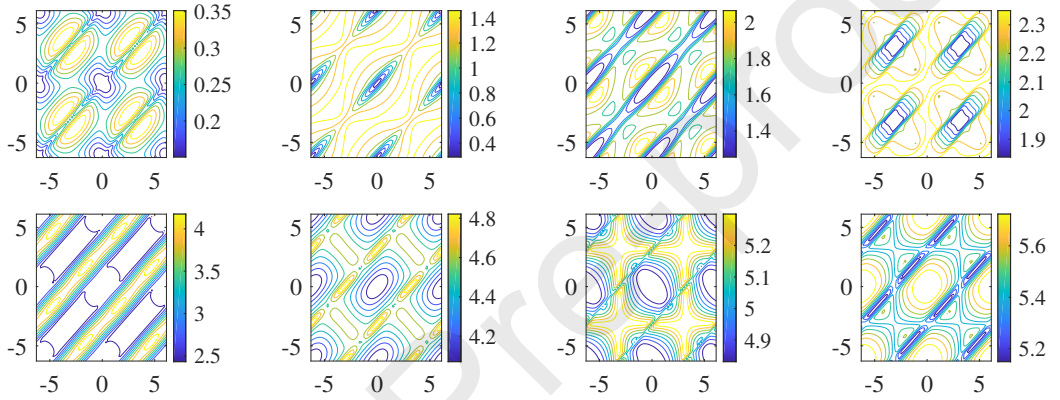

Figure 9: The effect of attached point masses on the iso-frequency contours of re-entrant $\theta = -10°$ lattice with additional point masses $M_p = \frac{1}{2}\rho AL$.

dispersion branches significantly. In other words, the stiffness of the elastic medium reduces the effects of pre-load on the band structure of the proposed lattice systems. Moreover, by setting the optimal values of the pre-load and stiffness of the elastic medium, one can control the stop and passbands of honeycomb structures, which can result in optimal design procedures of waveguides and filters. Here, there are no differences in a number and position of veering points for changes in the pre-load parameter in both lower and higher modes.

4.5. Dynamic behaviour of the embedded lattice structure

When investigating the free in-plane vibration of the whole lattice structure, size of the full FE model becomes large, which requires the application of model reduction techniques such as HCB method to reduce the problem. As stated above, the adopted model of the lattice is similar to a plate-like structure with corresponding boundary conditions. Here, we consider two types of boundary conditions the Free-Free-Free-Free (FFFF) and the Clamped-Free-Free-Free (CFFF), which represent the conditions at four sides of the plate i.e., boundary nodes. Dimensions of the plate are given as $L = 1.95$ m and $W = 2.1875$ m. For the application of HCB technique, the initial structure is divided into two sub-structures of lengths $L_1 = 0.97428$ m, and $L_2 = 0.97572$ m, while the height is equal to that of the initial structure. It should be emphasized that the interface reduction technique is based on the S-CC reduction discussed in Section 3. However, it is shown that since the interface consists of only the geometrical nodes, then S-CC reduction technique does not achieve satisfying accuracy compared to the HCB reduction method. Also, a comparative study has shown that the results obtained for natural frequencies by the presented HCB method and COMSOL Multiphysics software are in good agreement. However, the presented analysis does not perform any convergence study

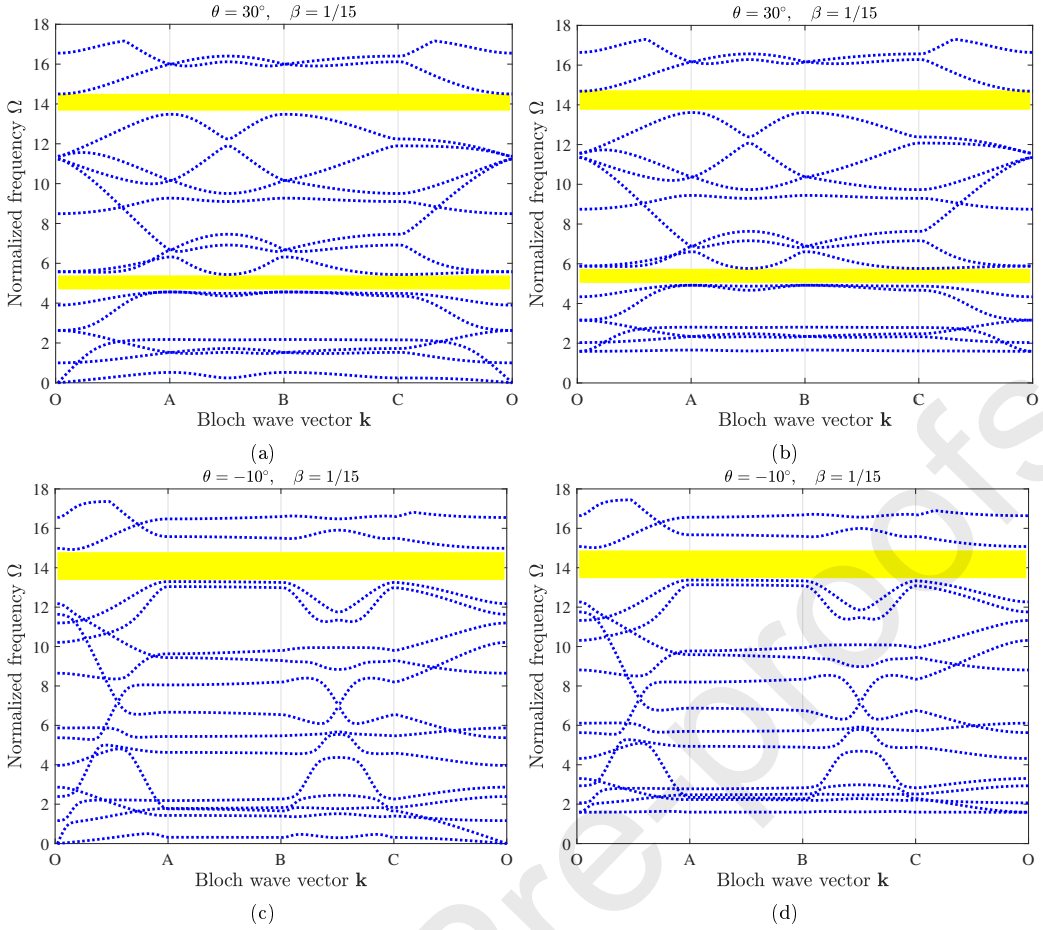

Figure 10: The effect of the Winkler's elastic medium on the frequency band structures determined for $N_0 = -10^4(N)$, $M_p = \frac{1}{12}\rho AL$, the regular hexagonal lattice, (a) $K_u = K_w = 0$ N/m^2; (b) $K_u = K_w = 10^8$ N/m^2; the re-entrant lattice, (c) $K_u = K_w = 0$ N/m^2; (d) $K_u = K_w = 10^8$ N/m^2.

of the reduced model, where maximum frequency and time errors are necessary for the eigenvalue analysis. For more details concerning these issues one is referred to [15, 59, 63].

4.6. Verification

To verify the results for the hexagonal plate-like structure obtained by the HCB model reduction and those from the interface reduction S-CC method, a comparative study is presented in Table 2 and Table 3 for two types of boundary conditions CFFF and FFFF. In this analysis, the effects of attached masses, pre-load, and stiffness of the Winkler's elastic medium are neglected. By solving the corresponding eigenvalue problem, the first ten natural frequencies are determined in Comsol Multiphysics software for the full model of a lattice structure and then compared with the results obtained by the HCB and S-CC model reduction techniques. Table 2 shows the results for natural frequencies given in (Hz) for the CFFF boundary conditions while Table 3 shows the results for the FFFF boundary conditions, where fine agreement between different approaches is achieved. It should be emphasized that the initial problem with 5655 and/or 4668 DOFs is reduced to the problem with only 133 DOFs by introducing the HCB model reduction technique. This significantly reduces the computational time in the dynamic analysis of large-scale problems such as honeycomb plate-like structures. Moreover, it is shown that the interface reduction technique achieves good results only for the first four natural frequencies, reducing the initial problem to only 115 DOFs. In the following parametric study, the influence of mass and stiffness matrices on the vibration behaviour of the lattice structure is investigated by the HCB model reduction technique.

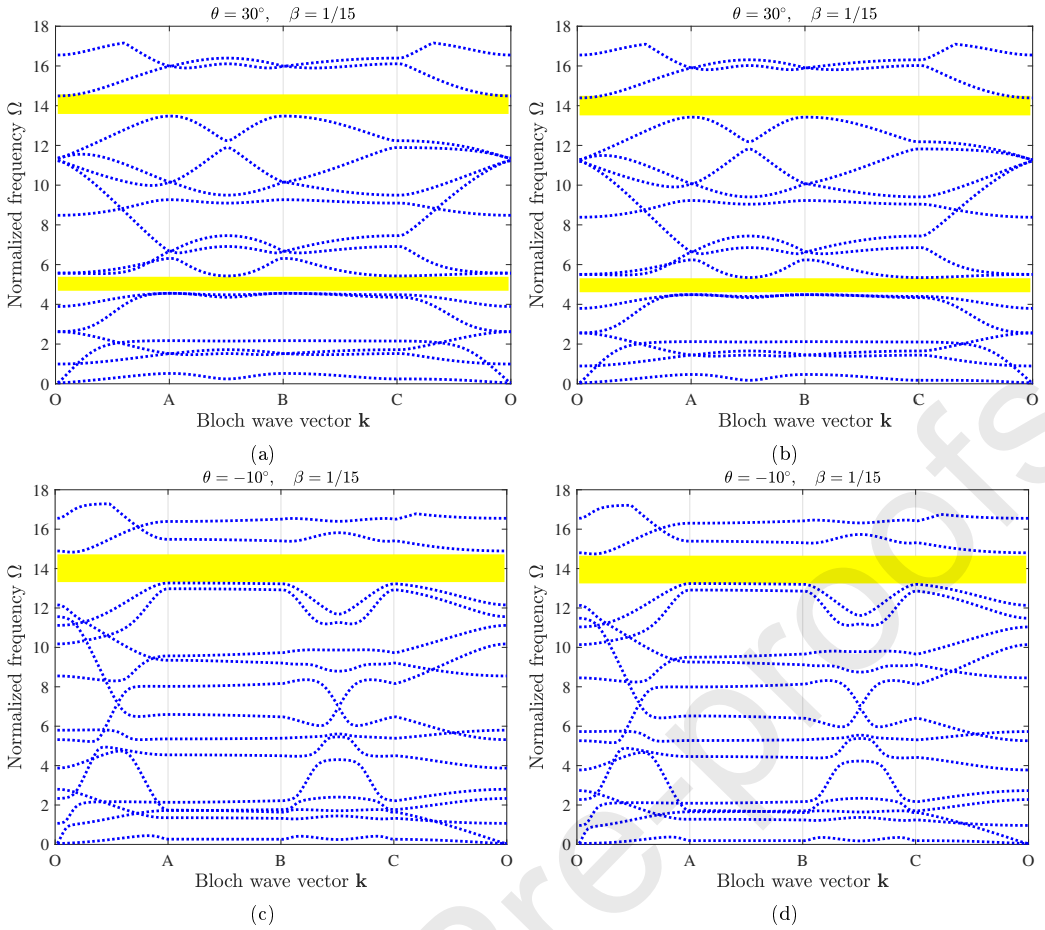

Figure 11: The effect of the pre-load on the frequency band structures determined for $K_u = K_w = 10^5$ N/m^2, $M_p = \frac{3}{12}\rho AL$, and the regular hexagonal lattice, (a) $N_0 = 0$ N; (b) $N_0 = 10^4$ N; the re-entrant lattice, (c) $N_0 = 0$ N; (d) $N_0 = 10^4$ N.

Table 2: The verification of natural frequencies Hz of the embedded hexagonal structure for CFFF boundary conditions ($K_w = K_u = M_p = N_0 = 0$). The number of finite elements per length L is $n_{ele} = 5$.

No.	COMSOL Multiphysics (full model 5655 DOFs)	Full model - CFFF 4638 DOFs	HCB reduction 133 DOFs	HCB+(S-CC) reduction 115 DOFs
1	17.197	17.201	17.202	17.335
2	44.822	44.832	44.837	46.838
3	46.593	46.603	46.604	48.781
4	71	71.014	71.016	73.348
5	73.941	73.958	73.986	92.792
6	86.489	86.501	86.519	104.42
7	92.385	92.406	92.429	107.59
8	100.7	100.71	100.81	121.2
9	116.66	116.69	116.8	125.52
10	118.71	118.73	119.03	132.73

4.7. The effects of system parameters on eigenvalue curves

In this subsection, the natural frequencies are determined by using the reduced mass and stiffness matrices obtained by the HCB reduction method for both CFFF and FFFF boundary conditions, represented as the eigenvalue curves. Fig.12 shows the effect of Winkler's elastic medium stiffness on the first ten natural frequencies. The magnitude of the stiffness is changed in the range 0 - 10^5 N and it is equal in both directions $k_u = k_w$. The obtained results reveal that an increase in the stiffness increases natural frequencies for both boundary conditions. However, it is evident that the influence of the medium's stiffness is more pronounced for CFFF boundary conditions than for the FFFF one, as given in Fig.12 (a). On the other hand, the impact of stiffness on the eigenvalue curves is almost linear for the FFFF boundary conditions as observed from Fig.12 (b). It is interesting to note

Table 3: The verification of natural frequencies Hz of the embedded hexagonal structure for FFFF boundary conditions ($K_w = K_u = M_p = N_0 = 0$). The number of finite elements per length L is $n_{ele} = 5$.

No.	COMSOL Multiphysics (full model 5655 DOFs)	Full model - FFFF 4668 DOFs	HCB reduction 133 DOFs	HCB+(S-CC) reduction 115 DOFs
1	59.472	59.486	59.505	60.949
2	63.517	63.53	63.586	64.108
3	66.987	67.003	67.012	70.089
4	68.031	68.046	68.062	79.466
5	74.716	74.729	74.731	86.41
6	89.241	89.252	89.304	92.272
7	90.298	90.31	90.321	97.246
8	94.306	94.326	94.372	109.86
9	98.317	98.339	98.365	116.93
10	111.39	111.41	111.44	122.19

that in general, the influence of elastic medium stiffness on higher natural frequencies is very low. Here, a frequency veering phenomenon can be observed from the modal analysis of the free in-plane vibration of the lattice structure, where the frequency is plotted in terms of system parameters. Here, no veering phenomenon can be detected on frequency curves for changes in stiffness of the Winkler's elastic medium.

The first ten natural frequencies in the form of eigenvalue curves with varying attached point masses for two different boundary conditions of the lattice structure are presented in Figure 13. The values of attached point masses are changed in the range 0 - 0.495 kg. It can be observed that an increase in the values of attached point masses can reduce the natural frequencies. Moreover, it can be seen that the natural frequencies determined for the FFFF boundary condition are more affected for the varying attached masses (refer Fig.13(b)), in comparison to the configuration with CFFF boundary conditions. However, in both cases one can notice a nonlinear relationship between the natural frequency and change of values of attached masses.

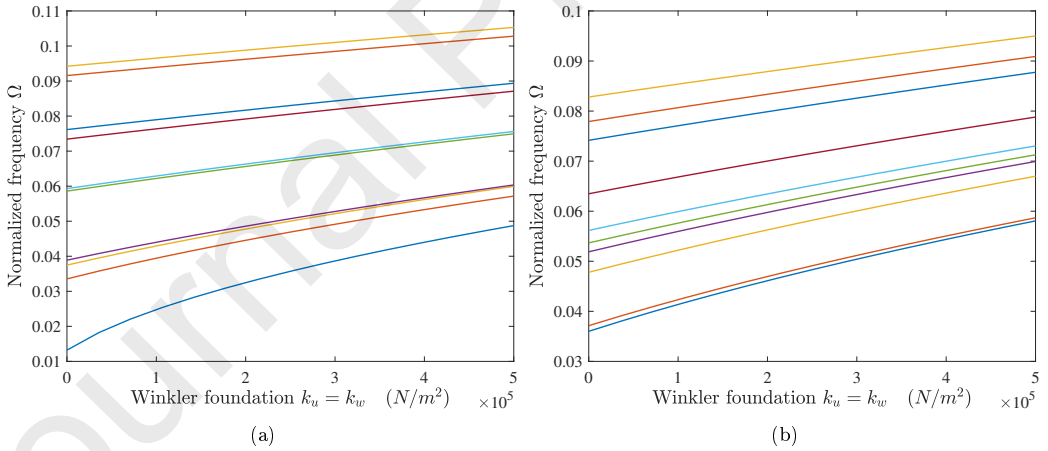

Figure 12: The effect of the stiffness of Winkler's elastic medium on natural frequencies for the embedded regular hexagonal structure $\theta = 30°$, with $N_0 = 10^4$ N, $M_p = \frac{3}{6}\rho AL$, $\beta = \frac{1}{10}$; (a) CFFF and (b) FFFF boundary conditions.

Further, Fig.14 shows the influence of the pre-load parameter, given in the range $-1.5 \cdot 10^4$ N $< N_0 < 1 \cdot 10^4$ N, on the first ten natural frequencies in form of eigenvalue curves for the lattice plate-like structure and two types of boundary conditions. In the previous two examples, we have seen that the influences of elastic medium stiffness and attached point masses on natural frequencies are almost identical for both boundary conditions. However, the pre-load directly influences the modes and corresponding natural frequencies. One can notice a frequency veering phenomenon for changes of the pre-load parameter. Fig.14 (a) depicts the natural frequencies determined for the plate-like lattice structure with CFFF boundary conditions. One can observe that the fourth, sixth, and eighth eigenvalues curves are having different behaviour for varying the preload parameter. At some points in the graph one can detect mode veering. Fig.14 (b) also shows an interesting behaviour of natural

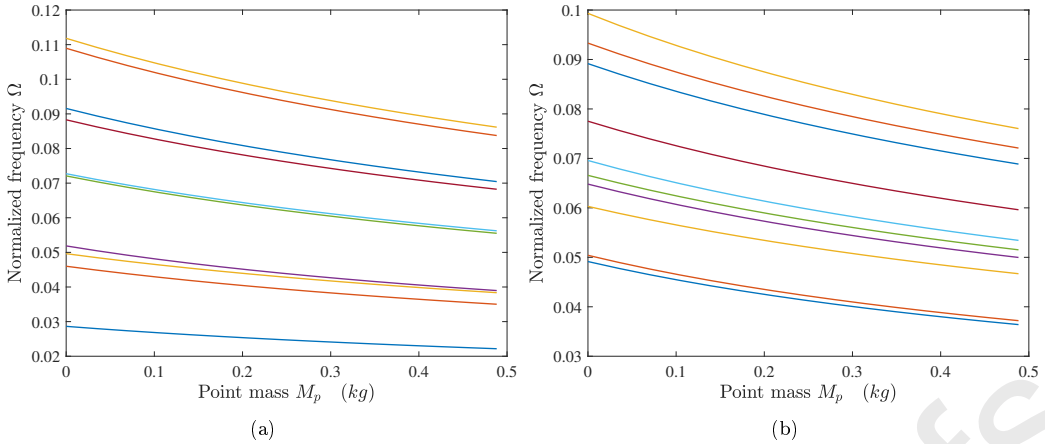

Figure 13: The effects of attached point masses on natural frequencies determined for the embedded regular hexagonal structure $\theta = 30°$, with $N_0 = 10^4$ N, $\beta = \frac{1}{10}$, $K_u = K_w = 10^5$ N/m^2; (a) CFFF and (b) FFFF boundary conditions.

frequencies obtained for the FFFF boundary conditions. In this case, one can also observe mode veering for varying values of the pre-load parameter. As mentioned before, plotted curves of natural frequencies in terms of varying pre-load parameter shows mode veering at certain points of the graph, which demonstrates the importance of this parameter for the appearance of this phenomenon.

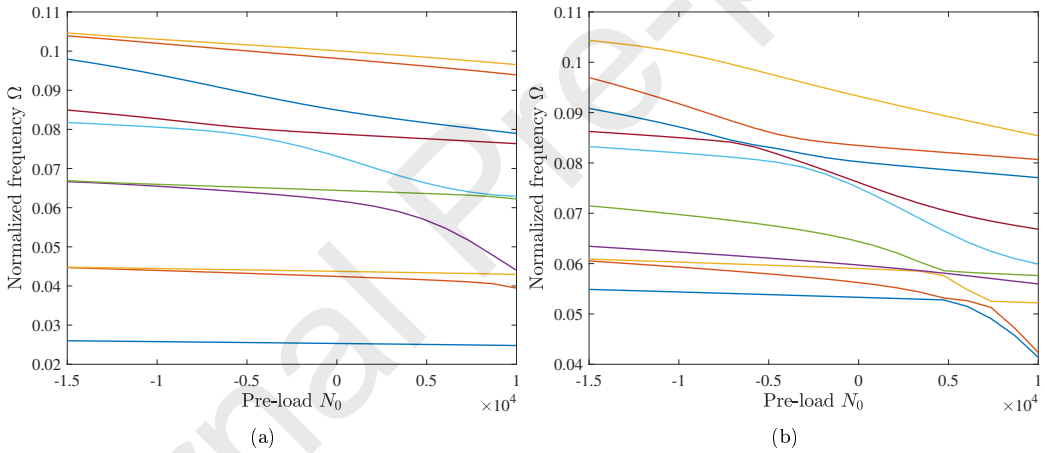

Figure 14: The effects of the pre-load on natural frequencies determined for the embedded regular hexagonal structure $\theta = 30°$, where $K_u = K_w = 10^5$ N/m^2, $M_p = \frac{3}{6}\rho AL$, $\beta = \frac{1}{10}$; (a) CFFF and (b) FFFF boundary conditions.

The last example shows the influence of the internal angle θ on the eigenvalue curves of the plate-like lattice system for two different boundary conditions, Fig.15. The natural frequencies in both boundary conditions are almost independent on the angle θ, except in the case when θ approaches the value of 30°. In 15 (a), for the case with CFFF boundary conditions, it can be noticed that the first natural frequency is almost unchanged for varying internal angle θ. However, at higher values of natural frequencies, multiple mode veering occur. On the other hand, the natural frequencies given in 15 (b) for the FFFF boundary conditions are manifesting slightly different behaviour since multiple veering occurs in a narrow frequency band. For this boundary condition case, natural frequencies demonstrate similar behaviour for changes of the internal angle θ. It can be concluded that lattice configuration has a strong impact on the appearance of veering phenomenon, which means it is sensitive to varying internal angle θ [74, 75]. Due to identical/close modes in periodic lattice structures, mode veering can also lead to mode degeneration/localization and should be investigated in the pre-design stage based on adequate dynamic models. According to [76], veering is manifested in dramatic changes of vibration modes with a strong impact on the dynamic response, which makes performed analyses crucial for insight into the dynamic behaviour of the presented hexagonal lattice

systems.

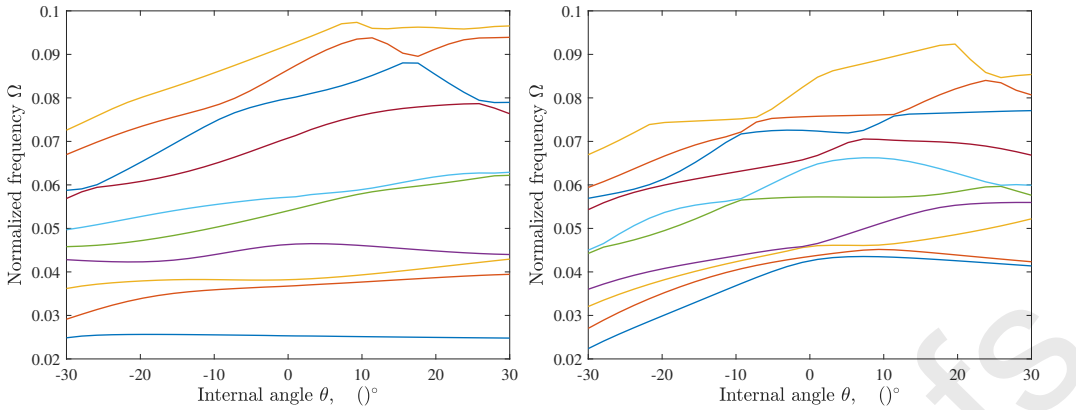

Figure 15: The effects of the internal angle θ on natural frequencies of the lattice structure for $K_u = K_w = 10^5$ N/m^2, $M_p = \frac{3}{6}\rho AL$, $N_0 = 10^4$ N, $\beta = \frac{1}{10}$; (a) CFFF and (b) FFFF boundary conditions.

5. Summary and Conclusions

The main contribution of this work lies in two aspects. First, it develops a generalized integrated equivalent cost-effective methodology which reduces the computational effort inherently associated with the analysis of wave propagation and dynamic behaviour of periodic lattice structures. In doing so, the proposed methodology efficiently blends in a two-tier physics-based model reduction strategy with the finite element method by coupling, (i) Bloch theorem for reducing the wave propagation analysis of lattice structures to that of a single unit cell, and (ii) Hurty-Craig-Bampton approach for reducing the internal and interface DOFs of the periodic lattice structures. Second, the emergence of frequency veering and zero-frequency band gap is detected in both wave propagation and vibration analysis of honeycomb lattice structures. This provides for the first time a framework to analyse this phenomenon from two different standpoints leading to results that shade into one another.

A model based on the finite element and Bloch wave analysis of the embedded and pre-stressed periodic lattice structure with attached point masses has been developed. Two types of lattice structures, namely, hexagonal and re-entrant honeycombs have been studied, with repetitive unit cells consisting of rigidly connected pre-stressed Timoshenko beams with attached point masses and embedded in the Winkler's type elastic medium. Dispersion curves have been generated by solving the corresponding eigenvalue problem and thereby, important information about band structures of the proposed lattice systems has been obtained. It is found that the combination of the attached point mass, pre-stress and Winkler's elastic medium significantly changes the band structure of lattice structures by introducing new band gaps at lower frequency branches including the zero-frequency band gap. Different veering points are noticed in regular and re-entrant lattice structures.

Dynamic behaviour of the finite length plate-like lattice structures has been investigated by comparing the full model and a reduced model using Hurty-Craig-Bampton approach with additional interface reductions. Comparison of the results for natural frequencies of the finite length lattice structure obtained in Comsol Multiphysics software for the full model and those obtained by using the model reduction techniques show fine agreement. Parametric study based on the reduced model demonstrated an interesting dynamic behaviour, especially for changes of the internal angle θ. The plots of natural frequency versus internal angle have shown multiple mode veering phenomena i.e., instances of mode degeneration/localization which can significantly affect the dynamic behaviour of a system. Mode veering has been observed for changes in the pre-load parameter. This is possibly the first reported observation of mode veering in lattice materials.

In conclusion, the proposed periodic lattice structures revealed exciting band structure and dynamic properties that make them prospective candidates for waveguides and filters. Moreover, the

introduction of attached point masses, pre-load and elastic medium is shown to be effective for tuning the band structure properties of lattice structures without changing the basic geometry of the system. These promising results can prove to be useful for adaptive/smart design of periodic lattice structures. The methods presented in this work can be used in future studies for application to more complex 3D lattice structures. Accounting for manufacturing variability in the proposed periodic structures is also another interesting topic of future research.

Acknowledgements

D. Karličić and S. Adhikari were supported by the Marie Skłodowska-Curie Actions - European Commission: 799201-METACTIVE. M. Cajić was sponsored by the Serbian Ministry of Education, Science and Technological Development and Mathematical institute of the Serbian Academy of Sciences and Art.

References

[1] A. S. Phani, M. I. Hussein, Dynamics of lattice materials, Wiley Online Library, 2017.
[2] V. Zalipaev, A. Movchan, C. Poulton, R. McPhedran, Elastic waves and homogenization in oblique periodic structures, Proceedings of the Royal Society of London. Series A: Mathematical, Physical and Engineering Sciences 458 (2024) (2002) 1887–1912.
[3] T. Mukhopadhyay, S. Adhikari, A. Batou, Frequency domain homogenization for the viscoelastic properties of spatially correlated quasi-periodic lattices, International Journal of Mechanical Sciences 150 (2019) 784–806.
[4] A. S. Phani, J. Woodhouse, N. Fleck, Wave propagation in two-dimensional periodic lattices, The Journal of the Acoustical Society of America 119 (4) (2006) 1995–2005.
[5] P. Martinsson, A. Movchan, Vibrations of lattice structures and phononic band gaps, Quarterly Journal of Mechanics and Applied Mathematics 56 (1) (2003) 45–64.
[6] C. Poulton, A. Movchan, R. McPhedran, N. Nicorovici, Y. Antipov, Eigenvalue problems for doubly periodic elastic structures and phononic band gaps, Proceedings of the Royal Society of London. Series A: Mathematical, Physical and Engineering Sciences 456 (2002) (2000) 2543–2559.
[7] S. Gonella, M. Ruzzene, Analysis of in-plane wave propagation in hexagonal and re-entrant lattices, Journal of Sound and Vibration 312 (1-2) (2008) 125–139.
[8] S. Mukherjee, F. Scarpa, S. Gopalakrishnan, Phononic band gap design in honeycomb lattice with combinations of auxetic and conventional core, Smart Materials and Structures 25 (5) (2016) 054011.
[9] J. Meng, Z. Deng, K. Zhang, X. Xu, Wave propagation in hexagonal and re-entrant lattice structures with cell walls of non-uniform thickness, Waves in Random and Complex Media 25 (2) (2015) 223–242.
[10] M. J. Leamy, Exact wave-based bloch analysis procedure for investigating wave propagation in two-dimensional periodic lattices, Journal of Sound and Vibration 331 (7) (2012) 1580–1596.
[11] F. Farzbod, M. J. Leamy, Analysis of bloch's method and the propagation technique in periodic structures, Journal of vibration and acoustics 133 (3) (2011).
[12] M. S. Mazloomi, M. Ranjbar, L. Boldrin, F. Scarpa, S. Patsias, N. Ozada, Vibroacoustics of 2d gradient auxetic hexagonal honeycomb sandwich panels, Composite Structures 187 (2018) 593–603.
[13] A. Glacet, A. Tanguy, J. Réthoré, Vibrational properties of quasi-periodic beam structures, Journal of Sound and Vibration 442 (2019) 624–644.
[14] X. An, H. Fan, C. Zhang, Elastic wave and vibration bandgaps in planar square metamaterial-based lattice structures, Journal of Sound and Vibration (2020) 115292.
[15] D. Krattiger, L. Wu, M. Zacharczuk, M. Buck, R. J. Kuether, M. S. Allen, P. Tiso, M. R. Brake, Interface reduction for hurty/craig-bampton substructured models: Review and improvements, Mechanical Systems and Signal Processing 114 (2019) 579–603.
[16] D. De Klerk, D. Rixen, S. Voormeeren, General framework for dynamic substructuring: History, review, and classification of techniques, AIAA Journal 46 (2008) 1169–1181.
[17] L. Boldrin, S. Hummel, F. Scarpa, D. Di Maio, C. Lira, M. Ruzzene, C. Remillat, T. Lim, R. Rajasekaran, S. Patsias, Dynamic behaviour of auxetic gradient composite hexagonal honeycombs, Composite Structures 149 (2016) 114–124.
[18] P. B. Silva, J. Mencik, J. R. D. F. Arruda, Wave finite element-based superelements for forced response analysis of coupled systems via dynamic substructuring, International Journal for Numerical Methods in Engineering 107 (6) (2016) 453–476.
[19] J. Mencik, A wave finite element approach for the analysis of periodic structures with cyclic symmetry in dynamic substructuring, Journal of Sound and Vibration 431 (6) (2016) 441–457.
[20] J. Fu, L. Xia, L. Gao, M. Xiao, H. Li, Topology optimization of periodic structures with substructuring, Journal of Mechanical Design 141 (7) (2019) 071403.

[21] X. Shiyin, H. Xiuchang, H. Hongxing, A study on the isolation performance of trichiral lattices with gradient geometry, Journal of Vibration and Control 21 (16) (2015) 3465–3475.
[22] C. Shen, G. Lu, T. Yu, Dynamic behavior of graded honeycombs–a finite element study, Composite structures 98 (2013) 282–293.
[23] S. Khakalo, V. Balobanov, J. Niiranen, Modelling size-dependent bending, buckling and vibrations of 2d triangular lattices by strain gradient elasticity models: applications to sandwich beams and auxetics, International Journal of Engineering Science 127 (2018) 33–52.
[24] E. Baravelli, M. Ruzzene, Internally resonating lattices for bandgap generation and low-frequency vibration control, Journal of Sound and Vibration 332 (25) (2013) 6562–6579.
[25] S. Gonella, M. Ruzzene, Homogenization and equivalent in-plane properties of two-dimensional periodic lattices, International Journal of Solids and Structures 45 (10) (2008) 2897–2915.
[26] L. Joseph, R. V. Craster, Asymptotics for rayleigh–bloch waves along lattice line defects, Multiscale Modeling & Simulation 11 (3) (2013) 871–889.
[27] M. Makwana, R. Craster, Homogenisation for hexagonal lattices and honeycomb structures, The Quarterly Journal of Mechanics and Applied Mathematics 67 (4) (2014) 599–630.
[28] R. K. Narisetti, M. Ruzzene, M. J. Leamy, Study of wave propagation in strongly nonlinear periodic lattices using a harmonic balance approach, Wave Motion 49 (2) (2012) 394–410.
[29] P. Wang, J. Shim, K. Bertoldi, Effects of geometric and material nonlinearities on tunable band gaps and low-frequency directionality of phononic crystals, Physical Review B 88 (1) (2013) 014304.
[30] D. Mousanezhad, S. Babaee, R. Ghosh, E. Mahdi, K. Bertoldi, A. Vaziri, Honeycomb phononic crystals with self-similar hierarchy, Physical Review B 92 (10) (2015) 104304.
[31] G. Trainiti, J. J. Rimoli, M. Ruzzene, Wave propagation in undulated structural lattices, International Journal of Solids and Structures 97 (2016) 431–444.
[32] K. Zhang, Y.-c. Su, X.-h. Hou, J.-m. Meng, Z.-c. Deng, Effect of pre-load on wave propagation characteristics of hexagonal lattices, Composite Structures 203 (2018) 361–372.
[33] M. Gei, Wave propagation in quasiperiodic structures: stop/pass band distribution and prestress effects, International journal of solids and structures 47 (22-23) (2010) 3067–3075.
[34] M. Gei, A. Movchan, D. Bigoni, Band-gap shift and defect-induced annihilation in prestressed elastic structures, Journal of Applied Physics 105 (6) (2009) 063507.
[35] M. Gei, D. Bigoni, A. Movchan, M. Bacca, Band-gap properties of prestressed structures, in: Acoustic metamaterials, Springer, 2013, pp. 61–82.
[36] M. Miniaci, M. Mazzotti, I. Bartoli, Modeling bloch waves in prestressed phononic crystal plates, Frontiers in Materials 6 (2019) 74.
[37] K. Zhang, P. Zhao, C. Zhao, F. Hong, Z. Deng, Study on the mechanism of band gap and directional wave propagation of the auxetic chiral lattices, Composite Structures 238 (2020) 111952.
[38] M. S. Anderson, Vibration of prestressed periodic lattice structures, AIAA journal 20 (4) (1982) 551–555.
[39] A. Koellner, M. Todt, G. Ganzosch, C. Völlmecke, Experimental and numerical investigation on pre-stressed lattice structures, Thin-Walled Structures 145 (2019) 106396.
[40] B. R. Mace, E. Manconi, Wave motion and dispersion phenomena: Veering, locking and strong coupling effects, The Journal of the Acoustical Society of America 131 (2) (2012) 1015–1028.
[41] K. Tee, A. Spadoni, F. Scarpa, M. Ruzzene, Wave propagation in auxetic tetrachiral honeycombs, Journal of Vibration and Acoustics 132 (3) (2010).
[42] A. E. Bergamini, M. Zündel, E. A. Flores Parra, T. Delpero, M. Ruzzene, P. Ermanni, Hybrid dispersive media with controllable wave propagation: A new take on smart materials, Journal of Applied Physics 118 (15) (2015) 154310.
[43] Z. Zhu, Z. Deng, S. Tong, B. Ding, J. Du, Elastic wave propagation in hierarchical lattices with convex and concave hexagons stacked vertexes, The Journal of the Acoustical Society of America 146 (3) (2019) 1519–1527.
[44] J. L. du Bois, S. Adhikari, N. A. J. Lieven, On the quantification of eigenvalue curve veering: A veering index, Transactions of ASME, Journal of Applied Mechanics 78 (4) (2011) 041007:1–8.
[45] C. Hodges, J. Woodhouse, Vibration isolation from irregularity in a nearly periodic structure: theory and measurements, The Journal of the Acoustical Society of America 74 (3) (1983) 894–905.
[46] H. C. Chan, J. K. Liu, Mode localization and frequency loci veering in disordered engineering structures, Chaos, Solitions and Fractals 11 (2000) 1493–1504.
[47] G. Happawana, A. Bajaj, O. Nwokah, A singular perturbation analysis of eigenvalue veering and modal sensitivity in perturbed linear periodic systems, Journal of Sound and Vibration 160 (2) (1993) 225–242.
[48] S. Natsiavas, Mode localization and frequency veering in a non-conservative mechanical system with dissimilar components, Journal of Sound and Vibration 165 (1) (1993) 137–147.
[49] S. Adhikari, Calculation of derivative of complex modes using classical normal modes, Computer and Structures 77 (6) (2000) 625–633.
[50] H. Jafari, M. H. Yazdi, M. M. S. Fakhrabadi, Damping effects on wave-propagation characteristics of microtubule-based bio-nano-metamaterials, International Journal of Mechanical Sciences (2020) 105844.
[51] T. Chatterjee, D. Karlic˘ic, S. Adhikari, M. Friswell, Gaussian process assisted stochastic dynamic analysis with applications to near-periodic structures, Mechanical Systems and Signal Processing 149 (2021) 107218.

[52] J. L. du Bois, S. Adhikari, N. A. J. Lieven, Mode veering in stressed framed structures, Journal of Sound and VibrationPublished online (2009).
[53] X. Liu, G. Hu, C. Sun, G. Huang, Wave propagation characterization and design of two-dimensional elastic chiral metacomposite, Journal of Sound and Vibration 330 (11) (2011) 2536–2553.
[54] L. Brillouin, Wave propagation in periodic structures: electric filters and crystal lattices (1953).
[55] J. N. Reddy, An introduction to the finite element method, New York 27 (1993).
[56] T. Yokoyama, Vibration analysis of timoshenko beam-columns on two-parameter elastic foundations, Computers & Structures 61 (6) (1996) 995–1007.
[57] C. Kittel, P. McEuen, P. McEuen, Introduction to solid state physics, Vol. 8, Wiley New York, 1996.
[58] E. Kaxiras, J. D. Joannopoulos, Quantum theory of materials.
[59] T. Chatterjee, S. Adhikari, M. Friswell, Uncertainty propagation in dynamic sub-structuring by model reduction integrated domain decomposition, Computer Methods in Applied Mechanics and Engineering 366 (2020) 113060.
[60] S. H. Boo, J. H. Kim, P. S. Lee, Towards improving the enhanced Craig-Bampton method, Computers and Structures 196 (2018) 63–75.
[61] H. A. Jensen, V. A. Araya, A. D. Muñoz, M. A. Valdebenito, A physical domain-based substructuring as a framework for dynamic modeling and reanalysis of systems, Computer Methods in Applied Mechanics and Engineering 326 (2017) 656–678.
[62] R. R. Craig, A. J. Kurdila, Fundamentals of structural dynamics, John Wiley & Sons, 2006.
[63] M. S. Allen, D. Rixen, M. van der Seijs, P. Tiso, T. Abrahamsson, R. L. Mayes, Substructuring in Engineering Dynamics, Springer, 2020.
[64] X. An, F. Sun, P. Yu, H. Fan, S. He, D. Fang, Negative effective mass density of one-dimensional hierarchical metacomposite, Journal of Applied Mechanics 82 (3) (2015).
[65] Y. Tian, J. H. Wu, H. Li, C. Gu, Z. Yang, Z. Zhao, K. Lu, Elastic wave propagation in the elastic metamaterials containing parallel multi-resonators, Journal of Physics D: Applied Physics 52 (39) (2019) 395301.
[66] R. K. Pal, M. I. Rosa, M. Ruzzene, Topological bands and localized vibration modes in quasiperiodic beams, New Journal of Physics 21 (9) (2019) 093017.
[67] P. Wang, F. Casadei, S. H. Kang, K. Bertoldi, Locally resonant band gaps in periodic beam lattices by tuning connectivity, Physical Review B 91 (2) (2015) 020103.
[68] A. J. Zelhofer, D. M. Kochmann, On acoustic wave beaming in two-dimensional structural lattices, International Journal of Solids and Structures 115 (2017) 248–269.
[69] W. Liu, J.-W. Chen, X.-Y. Su, Local resonance phononic band gaps in modified two-dimensional lattice materials, Acta Mechanica Sinica 28 (3) (2012) 659–669.
[70] S. Gonella, A. C. To, W. K. Liu, Interplay between phononic bandgaps and piezoelectric microstructures for energy harvesting, Journal of the Mechanics and Physics of Solids 57 (3) (2009) 621–633.
[71] S.-Y. Chang, C.-D. Chen, J.-Y. Yeh, L.-W. Chen, Elastic wave propagation of two-dimensional metamaterials composed of auxetic star-shaped honeycomb structures, Crystals 9 (3) (2019) 121.
[72] M. Ruzzene, F. Scarpa, F. Soranna, Wave beaming effects in two-dimensional cellular structures, Smart materials and structures 12 (3) (2003) 363.
[73] T. Zhang, Y. Cheng, J.-z. Guo, J.-y. Xu, X.-j. Liu, Acoustic logic gates and boolean operation based on self-collimating acoustic beams, Applied Physics Letters 106 (11) (2015) 113503.
[74] X. Liu, Behavior of derivatives of eigenvalues and eigenvectors in curve veering and mode localization and their relation to close eigenvalues, Journal of Sound and Vibration 256 (3) (2002) 551–564.
[75] A. Gallina, L. Pichler, T. Uhl, Enhanced meta-modelling technique for analysis of mode crossing, mode veering and mode coalescence in structural dynamics, Mechanical systems and signal processing 25 (7) (2011) 2297–2312.
[76] J. Lin, R. G. Parker, Natural frequency veering in planetary gears, Mechanics of Structures and Machines 29 (4) (2001) 411–429.

Appendix 1: The shape function and matrix coefficients

The adopted shape functions of the Timoshenko beam element:

$$\Gamma_1(x) = 1-\xi, \quad \Gamma_2(x) = 0, \quad \Gamma_3(x) = 0, \tag{39}$$
$$\Gamma_4(x) = \xi, \quad \Gamma_5(x) = 0, \quad \Gamma_6(x) = 0,$$

$$\Lambda_1(x) = 0, \quad \Lambda_2(x) = \frac{1-3\xi^2+2\xi^3+(1-\xi)\Phi}{1+\Phi}, \quad \Lambda_3(x) = \frac{h_e(\xi-2\xi^2+\xi^3+\frac{1}{2}(\xi-\xi^2)\Phi)}{1+\Phi}, \tag{40}$$
$$\Lambda_4(x) = 0, \quad \Lambda_5(x) = \frac{3\xi^2-2\xi^3+\xi\Phi}{1+\Phi}, \quad \Lambda_6(x) = \frac{h_e(-\xi^2+\xi^3-\frac{1}{2}(\xi-\xi^2)\Phi)}{1+\Phi},$$

$$\Theta_1(x) = 0, \quad \Theta_2(x) = \frac{6(-\xi + \xi^2)}{h_e(1+\Phi)}, \quad \Theta_3(x) = \frac{1 - 4\xi + 3\xi^2 + (1-\xi)\Phi}{1+\Phi}, \tag{41}$$

$$\Theta_4(x) = 0, \quad \Theta_5(x) = \frac{6(\xi - \xi^2)}{h_e(1+\Phi)}, \quad \Theta_6(x) = \frac{-2\xi + 3\xi^2 + \xi\Phi}{1+\Phi},$$

where $\xi = x/h_e$ is the dimensionless axial coordinate and $\Phi = \frac{12EI}{GAk_s h_e^2}$ is the shear deformation parameter.

The elements of the mass and stiffness matrices for finite element beam model:

$$K_{ij}^e = \int_0^{h_e} \left[EA\frac{\partial \Gamma_i}{\partial x}\frac{\partial \Gamma_j}{\partial x} + EI\frac{\partial \Theta_i}{\partial x}\frac{\partial \Theta_j}{\partial x} + GAk_s\left(\Theta_i - \frac{\partial \Lambda_i}{\partial x}\right)\left(\Theta_j - \frac{\partial \Lambda_j}{\partial x}\right) \right.$$
$$\left. + k_w \Lambda_i \Lambda_j + k_u \Gamma_i \Gamma_j - N_0 \frac{\partial \Lambda_i}{\partial x}\frac{\partial \Lambda_j}{\partial x} \right] dx, \tag{42}$$

$$M_{ij}^e = \int_0^{h_e} \left(\rho A \Gamma_i \Gamma_j + \rho I \Theta_i \Theta_j + \rho A \Lambda_i \Lambda_j\right) dx, \tag{43}$$

$$R_{ij}^e = \int_0^{h_e} \left(\sum_{p=1}^{M} M_p \delta(x - a_p) \Gamma_i \Gamma_j + \sum_{p=1}^{M} M_p \delta(x - a_p) \Lambda_i \Lambda_j \right) dx, \tag{44}$$

where matrix $\mathbf{R}^e$ represents the additional mass matrix due to attached point masses on the beam.